High-Resolution Airborne Microwave Imaging of Snow Cover and Snow Water Equivalent (SWE) Retrieval

Boba Stankov[1], Al Gasiewski[2], Don Cline[3], Bob Weber[2], Gary Wick[1], and Marco Tedesco[5]

[1] NOAA Earth Systems Research Laboratory, Boulder, CO, USA
[2] University of Colorado, Center for Environmental Technology Laboratory, Boulder, CO USA,
[3] NOAA/NWS/National Operational Hydrologic Remote Sensing Center, Chanhassen, MI, USA
[5] NASA Goddard Space Flight Center, Greenbelt, MD, USA

Based on paper submitted to TGARS:
"High-Resolution Airborne Polarimetric Microwave Imaging of Snow Cover During the NASA Cold Lands Processes Experiment (CLPX)",
by B. B. Stankov, A.J. Gasiewski, D. Cline, B. L. Weber, G. A. Wick, and M. Klein

and on the IGARSS07 Conference Proceedings paper:
" Empirical SWE retrieval using airborne microwave and in situ snow measurements",
by B. B. Stankov, D. Cline, and M. Tedesco.

Introduction

Cold land regions play a critical role in the Earth's hydrologic cycle and have a significant impact on global weather and climate through their modulation of the Earth's radiation budget, storage of greenhouse gases in frozen tundra, and moderation of boundary layer fluxes.

Here we examine the response of microwave brightness temperature (T_B) across a broad range of snowpack properties and explore empirical algorithms for retrieval of snow water equivalent (SWE).

Talk Outline:

- Theory (Chang 1986).
- Cold Lands Processes Experiment (CLPX) 2002-2003.
- Polarimetric Scanning Radiometer (PSR) data analysis, surface emissivity calculation, and the resulting surface emissivity images for the 6.9, 10.7, 18.7, 21.5, 37, and 89 GHz microwave channels.
- Validation using ground-based data and the semi-empirical model data.
- Development of the regional retrieval algorithm.
- Comparison with Advanced Microwave Scanning Radiometer for EOS (AMSR-E) measurements.
- Summary

Theory

Theoretical Microwave Frequency Dependence on SWE

Theory indicates that:

- Scattering of upwelling microwave radation is sensitive to physical properties of dry snowpacks, particularly to depth, and density (together=SWE), and grain size.
- Scattering increases nonlinearly with increasing frequency, SWE, and grain size;

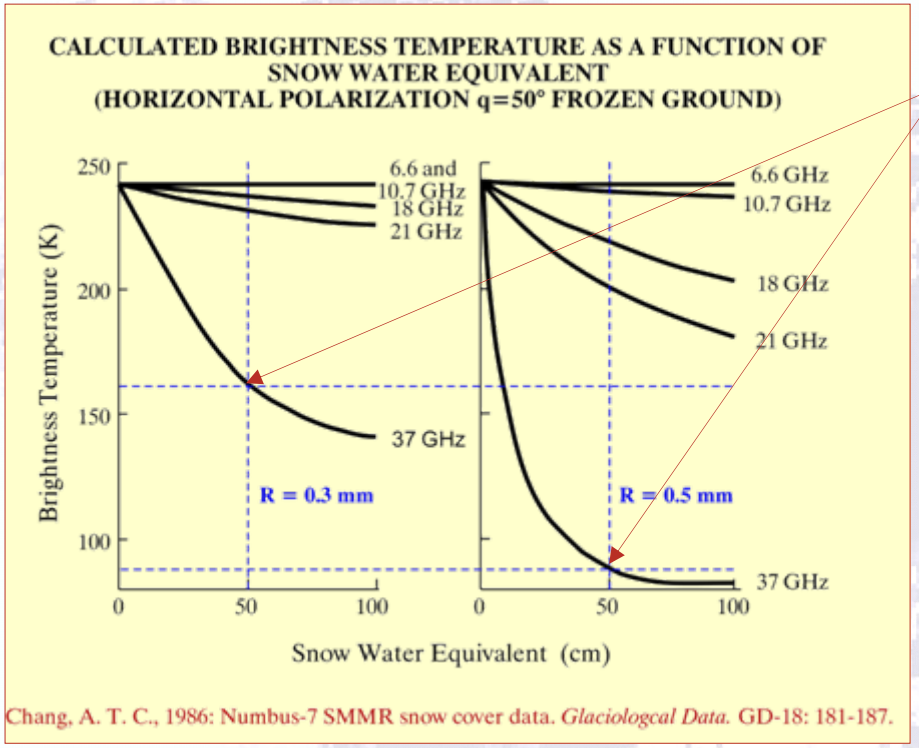

Chang, A. T. C., 1986: Numbus-7 SMMR snow cover data. *Glaciologcal Data.* GD-18: 181-187.

- The theoretical effect of snow grain size is large — an increase in the particle radius from R=0.3 to R=0.5 mm results in a T_B drop of ~70 K.
- The 37 GHz response becomes insensitive to further increases in SWE beyond 1 m, therefore this is the upper limit of this approach.

This theoretical dependence has been exploited to retrieve SWE using spaceborne radiometers for more than 20 years now.

Using $\Delta T_B=(T_{B18}-T_{B37})$ GHz difference, Chang 1986 developed the classical algorithmic approach by linearly fitting data in the figure and assuming a snow density of 300 kg/m^3.

Actual Microwave Frequency Dependence on SWE

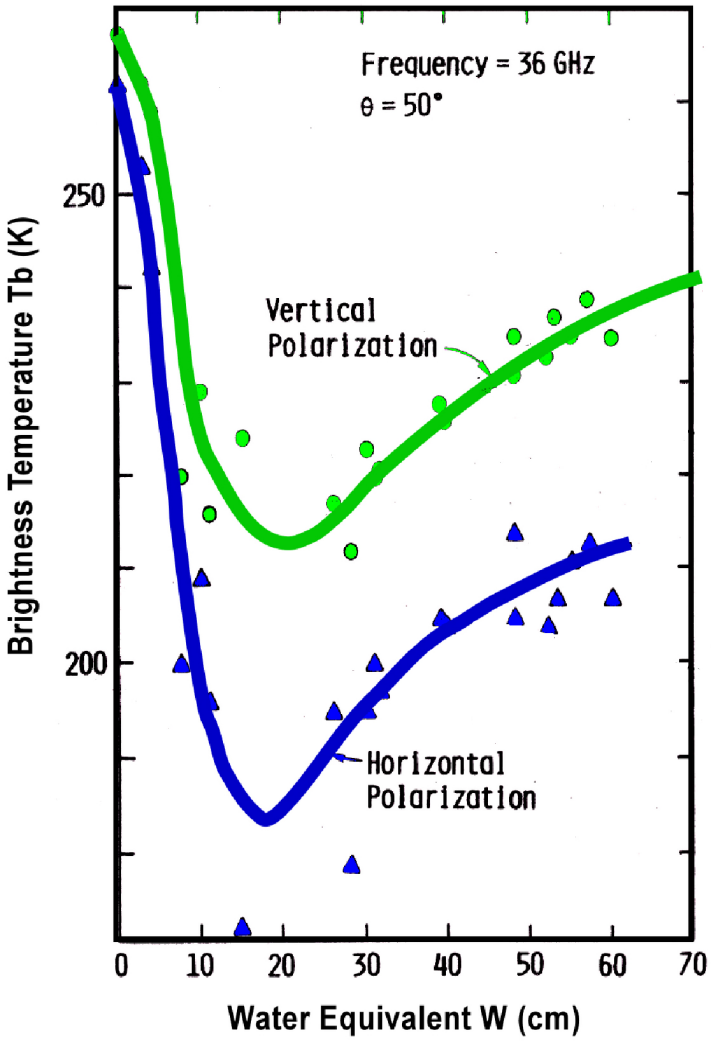

- T_B is also sensitive to other snow and underlying ground parameters, so the T_B dependence on SWE does not resemble the smooth theoretically derived curves.
- Natural snowpacks usually contain layers with varying density, grain size, and shape distributions, as well as buried ice lenses or crusts.
- Snowpacks undergo metamorphism whereby the size and shape of snow grains evolve over time.
- Consequently, independent of SWE, any snowpack may exhibit a wide range of microwave response as it evolves.

Thus, the limitations of using generalized theoretical response functions for global SWE retrieval are evident.

Schanda, E., Matzler C., and Kunzi K. (1983), Microwave Remote Sensing of Snow Covers. Int. J. Remote Sensing, 4, 149-158.

Cold Lands Processes Experiment (CLPX)

Cold Land Processes Experiments

To improve SWE observing capabilities and advance understanding of cryospheric processes, NASA Terrestrial Hydrology and the Earth Observing System Programs sponsored the multi-institutional Cold Land Processes Experiment.

- Spatially intensive *in situ* measurements of snowpack properties were collected over a wide range of snow conditions in February 2002 and February and March 2003.
- Coincident high-resolution measurements of surface brightness temperature (T_B) were collected from aircraft using the NOAA Polarimetric Scanning Radiometer (PSR)*.

*Now part of the University of Colorado's Center for Environmental Technology (CET)

CLPX 2002-2003 Site

Seven flight lines covered each mesoscale study area (MSA)

Each MSA contained three 1x1-km intensive study areas (ISA) marked by X

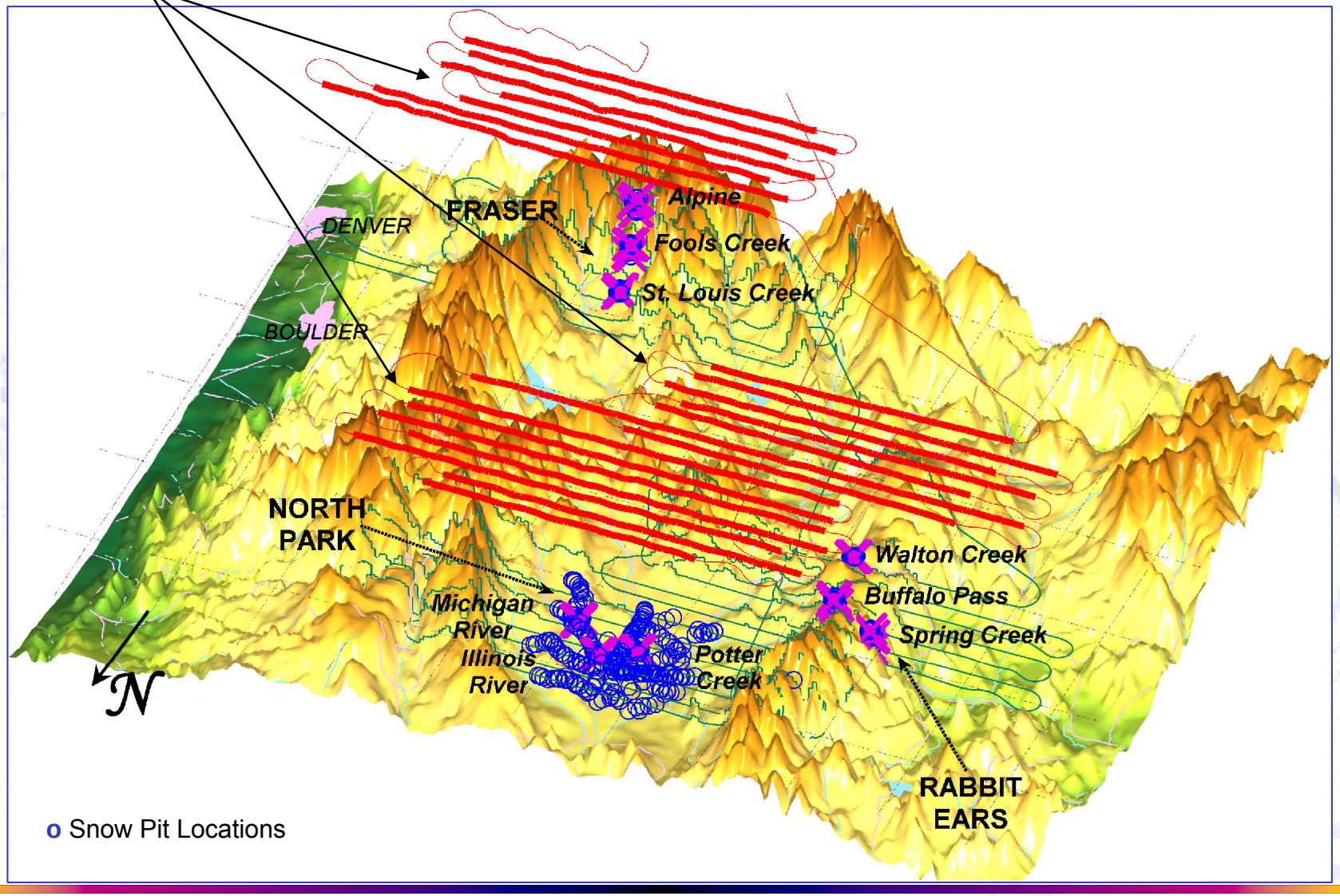

USGS 30-m Resolution Land Cover at Each MSA

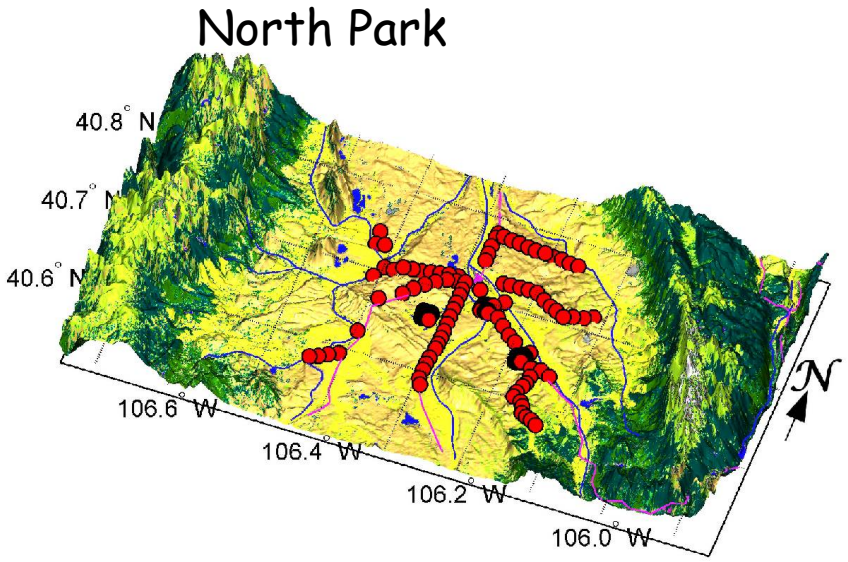

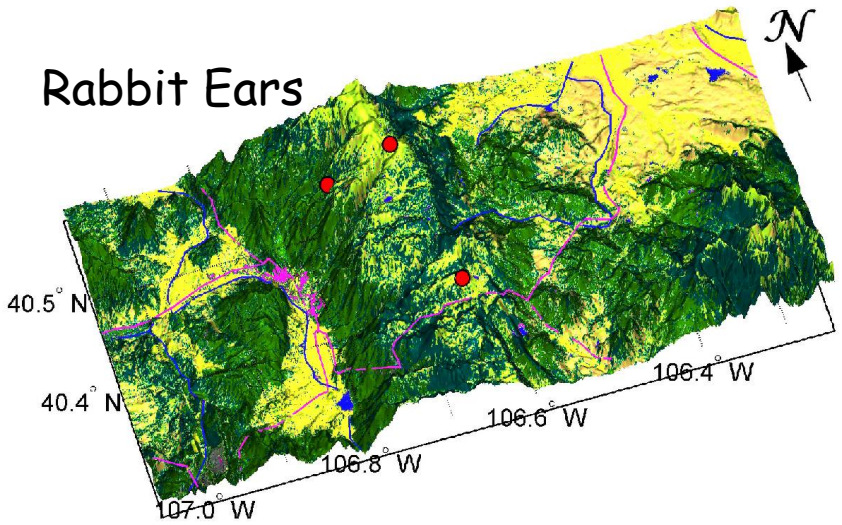

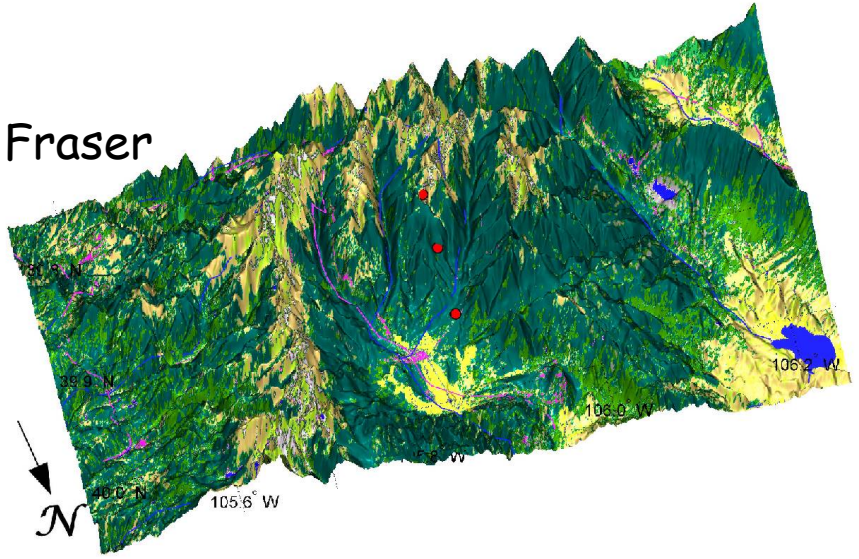

- Pasture and Row Crops
- Grass
- Shrubs
- Mixed Forest
- Coniferous Forest
- Deciduous Forest
- Barren Land
- Residential
- Perennial Ice and Snow
- Water

● Locations of the ground-based observations

Ground-based observations at ISAs

North Park

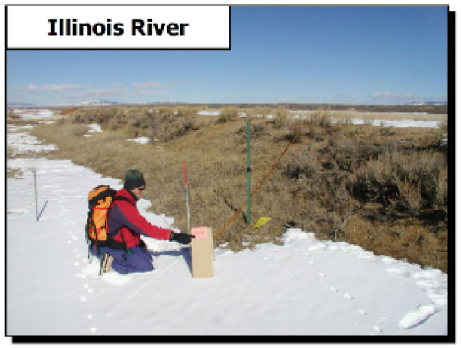

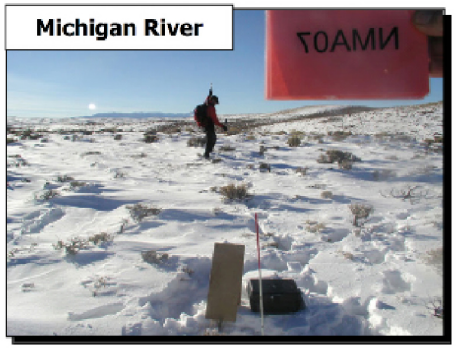

Rabbit Ears

Fraser

PSR Configuration

- The PSR is an airborne multi-band radiometer system with estimated nominal absolute accuracy of ±1 K for the range of T_B values encountered during CLPX.
- During CLPX the instrument was operated in a conical-scanning mode at an incidence angle of 55° from nadir.
- In February 2002 and 2003 PSR/A scanhead with 10.7, 18.7, 21.5, 37, and 89 GHz channels was used.
- In March 2003 the PSR/CXI scanhead with 5.8-7.5 GHz microwave band was added to the PSR/A scanhead for full polarimetric and spectral simulation of AMSR-E.

PSR Configuration During CLPX

	CLPX02	CLPX03A	CLPX03B
Aircraft	DC8	P-3	P-3
Scanhead	PSR/A	PSR/A	PSR/A PSR/CX

Total flight hours = 29.7
Number of flight lines = 154

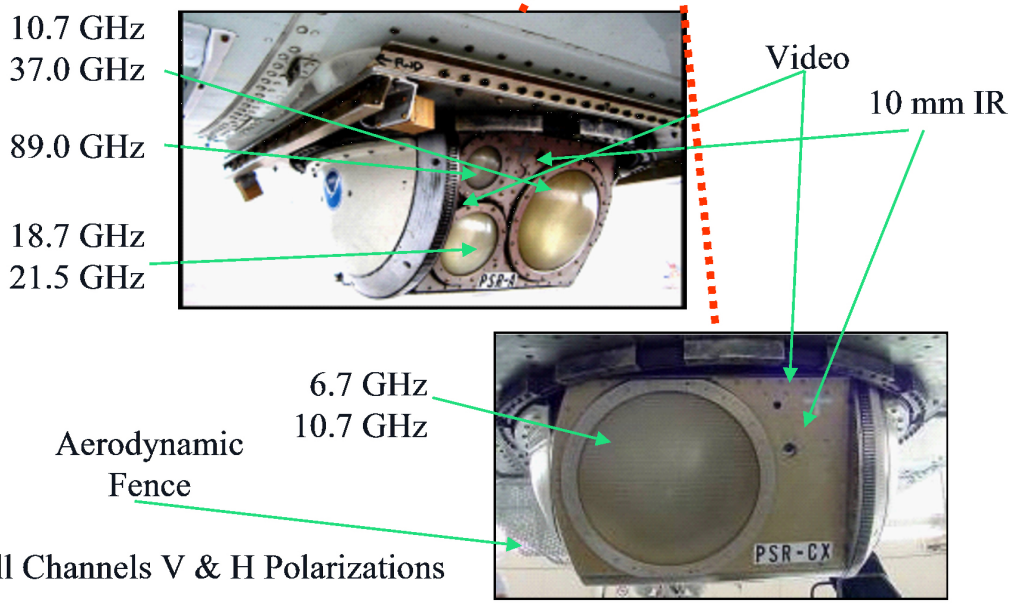

Spatial resolution range for 37 and 89 GHz channel = 80 - 226 m
Spatial resolution range for 10.7, 18.7, 21.5 Ghz channel = 272-787 m

CLPX 2002-2003 Weather

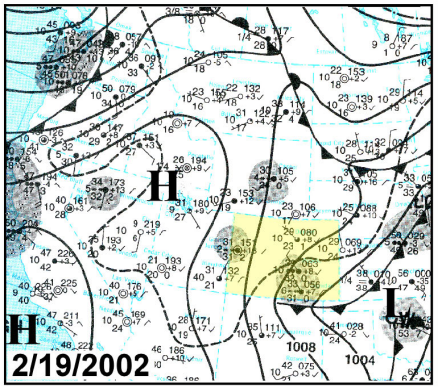

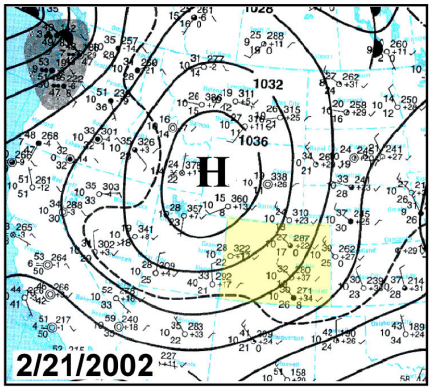

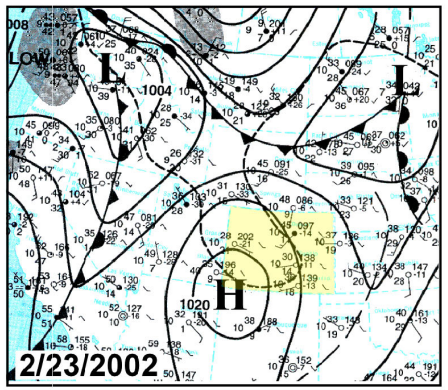

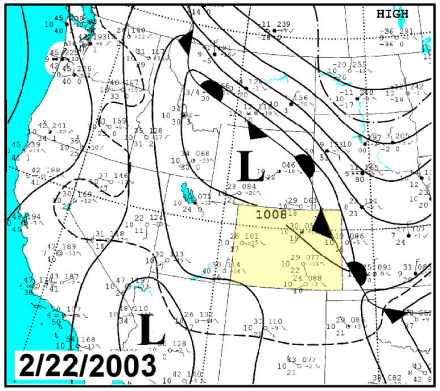

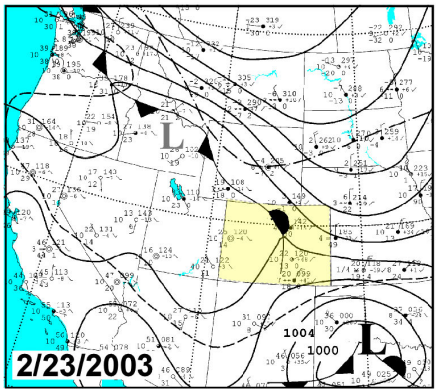

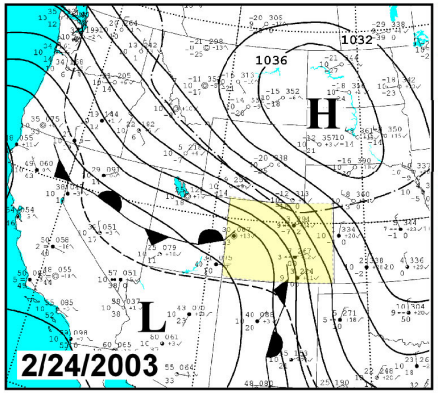

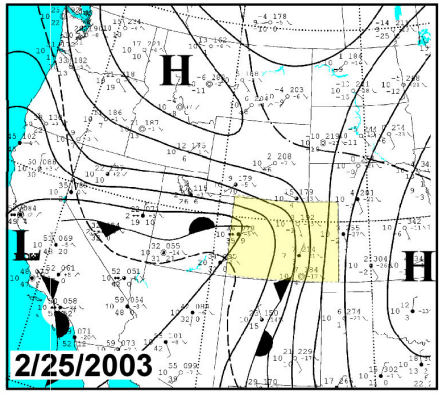

During 16-20 March 2003 period an extreme snowfall event with up to 2.2-m accumulation occurred over the southern Rocky Mountains and the High Plains region.

It is believed that such an event occurs only once per 100 year.

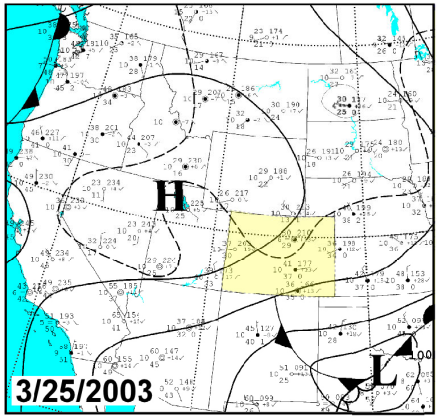

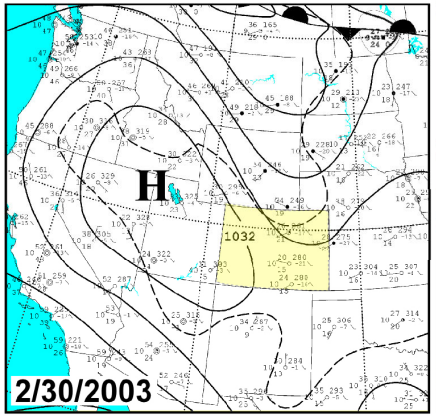

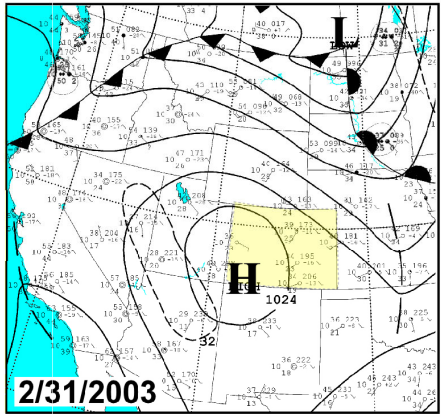

CLPX 2002-2003 3-hourly NARR

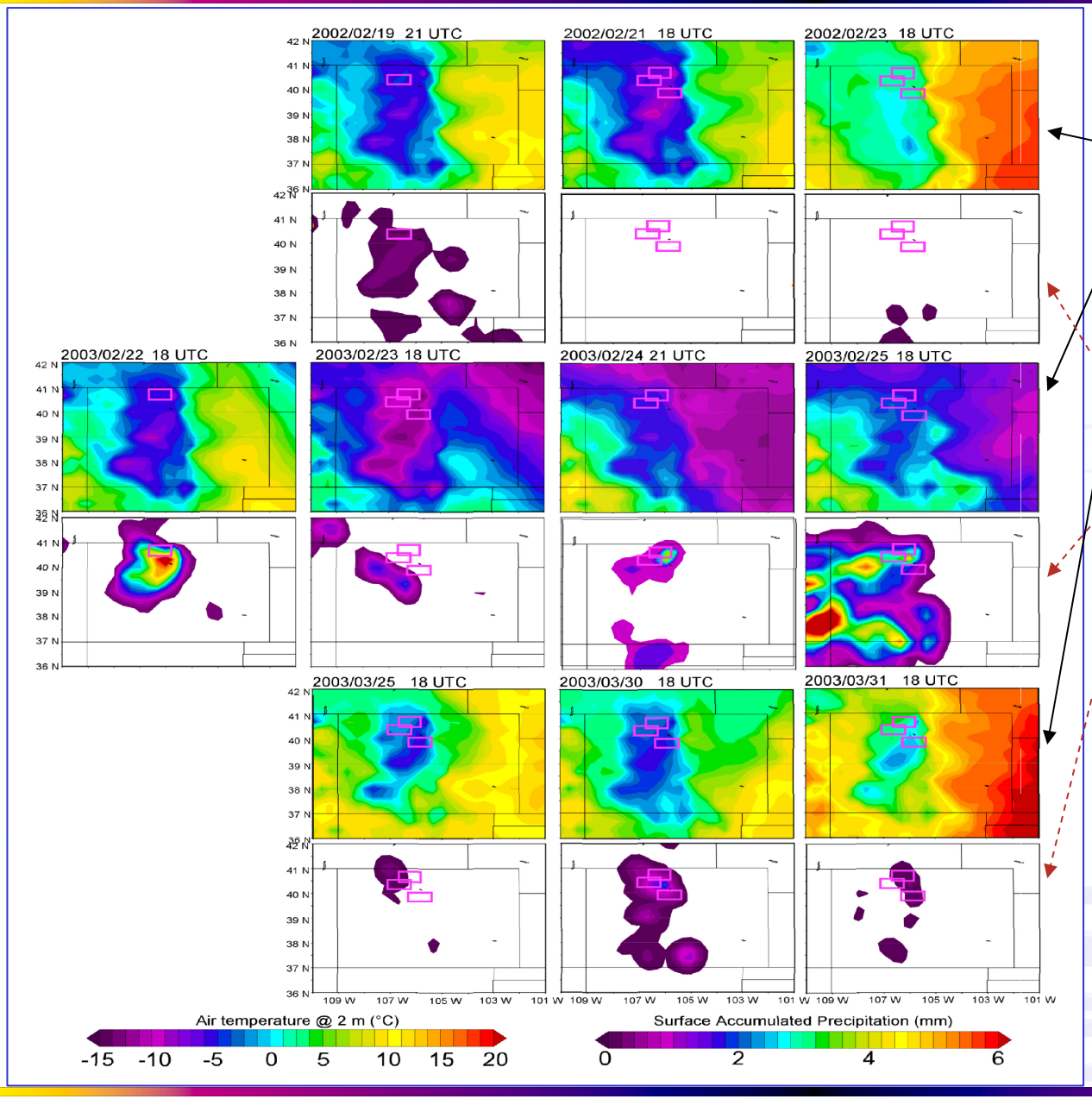

Air Temperature at 2-m AGL in °C

Surface Accumulated Precipitation during the previous 3-h in (mm)

PSR Data Analysis

Motivation for Data Analysis

PSR/A L2.3G 89.0 GHz T_v March 25, 2003 Imagery:

CL3B.DF001.C0100+0101+0102+0103+0104+0105+0107.SLM.* - Scans 1 to 1216 - Conical

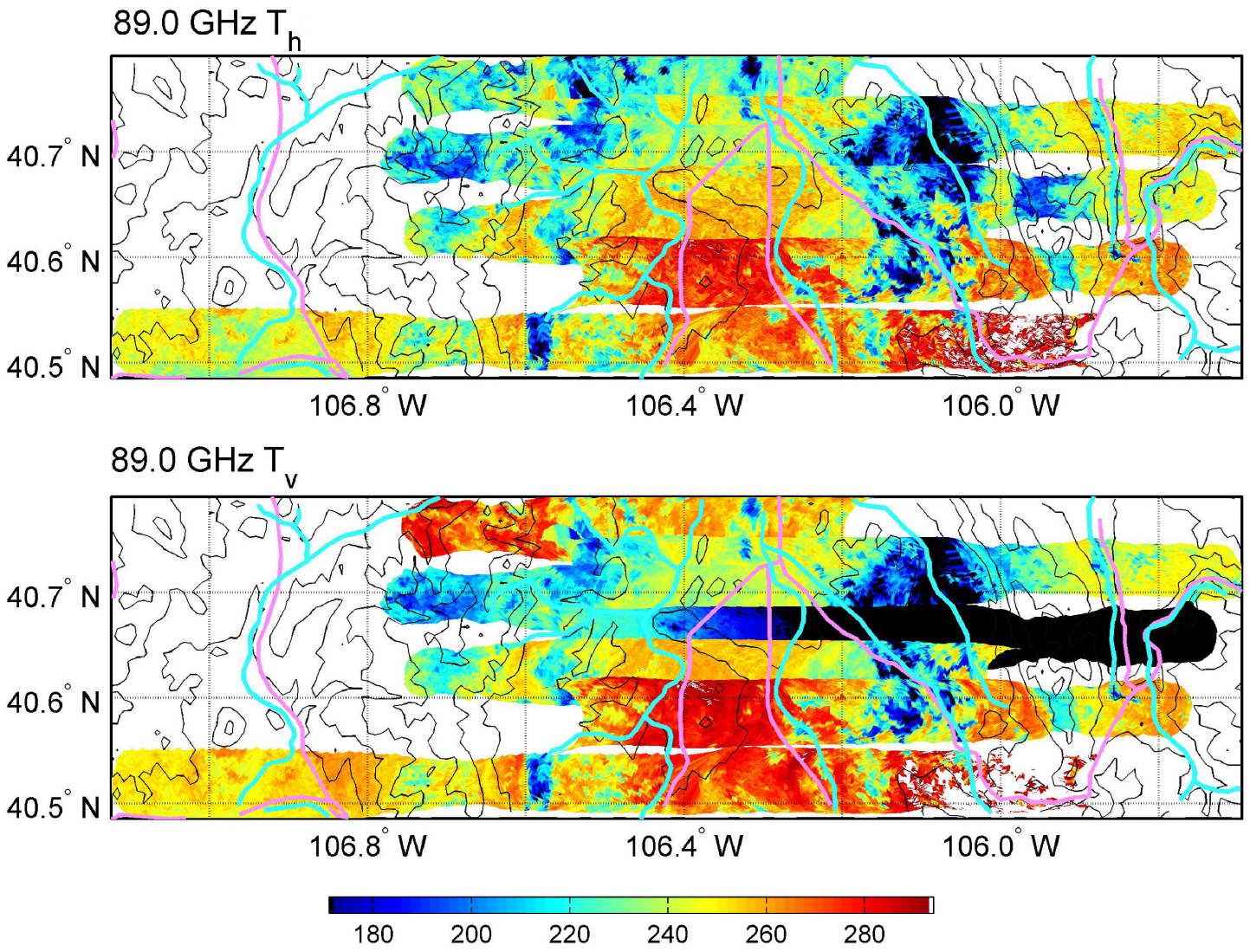

RT Calculation of Surface Emissivity

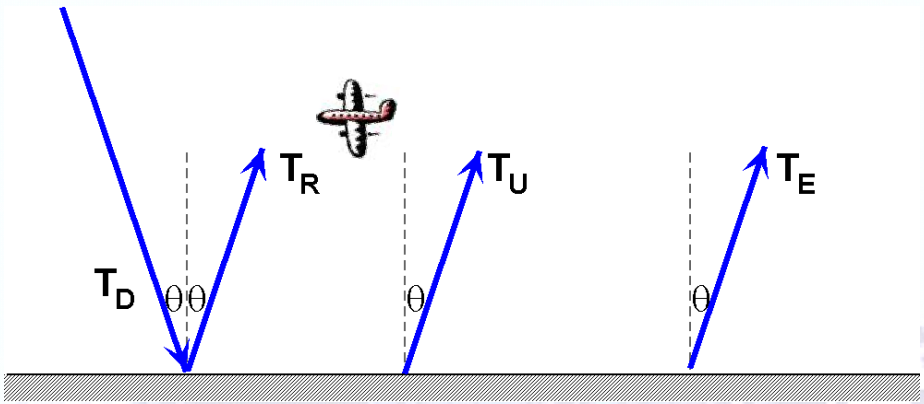

$$T_B = T_R + T_U + T_E$$

$T_B =$	brightness temperature at aircraft observation level
T_D	due to downwelling at the surface
$T_R = T_D(1-\varepsilon_S)e^{-\tau \sec\theta}$	due to reflection at the surface of downwelling radiation
T_U	due to upwelling
$T_E = \varepsilon_S T_S e^{-\tau \sec\theta}$	due to surface emission
T_S	surface temperature
$\tau =$	optical depth from surface to observation level

RT Calculation of Surface Emissivity

ε_S = surface emissivity (H- or V-polarization)

$$T_B = T_D\left(1-\varepsilon_S\right)e^{-\tau\sec\theta} + T_U + \varepsilon_S T_S e^{-\tau\sec\theta}$$

Solving for surface emissivity gives :

PSR

MRT*

$$\varepsilon_S = \frac{\left(T_B - T_U\right)e^{\tau\sec\theta} - T_D}{\left(T_S - T_D\right)}$$

PSR IR/
LAPS T_g

* MRT using NWS RAOBs augmented by surface observations from NCAR flux tower (Mahrt et al.)

RT Calculation of Surface Emissivity

To obtain surface temperature data the PSR IR sensor data and the LAPS ground temperature interpolated to the PSR measurement locations were used. Cloudy conditions were accounted for by always selecting the higher of the two values.

Atmospheric soundings used in the RT calculation were a composite of four adjacent RAOB profiles from Grand Junction and Denver. To account for the terrain elevation difference we used NCAR flux tower surface measurements at the North Park MSA.

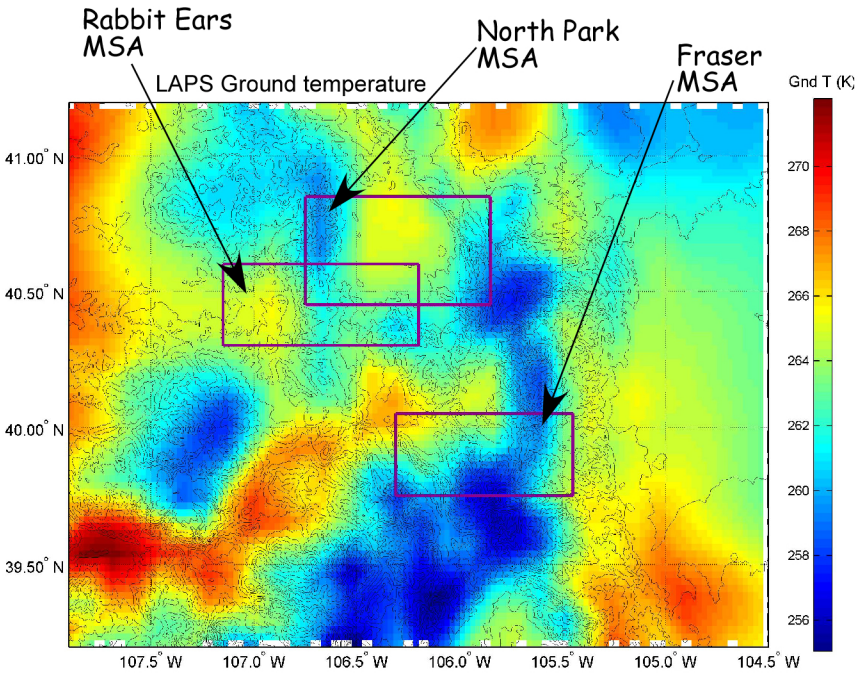

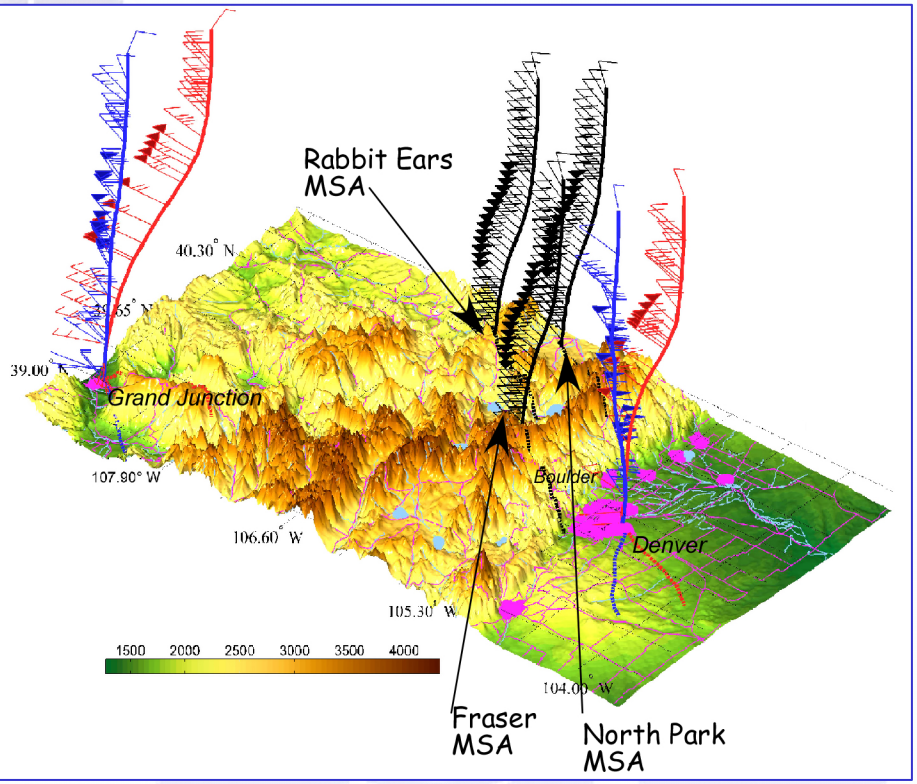

PSR Footprint Adjustment with Respect to Terrain 26

Geo-Gegistration

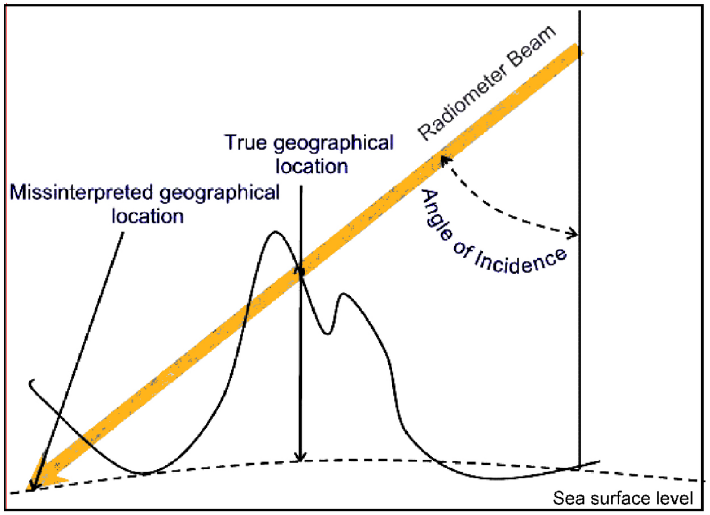

- Ray-tracing geolocation procedure was used because of the mountainous terrain.
- We used USGS 30-m resolution terrain elevation data to locate points where PSR beams intersected the surface.
- Vector normal to the terrain facet was computed and saved during the implementation of the geolocation procedure.

Re-projection

In the presence of terrain, the surface emissivity for horizontal polarization ε'_{Sh} and the surface emissivity for vertical polarization ε'_{Sv} are related to the PSR polarization measurements as follows:

$$\varepsilon'_{Sh} = \varepsilon_{Sv} \sin^2 \alpha + \varepsilon_{Sh} \cos^2 \alpha$$

$$\varepsilon'_{Sv} = \varepsilon_{Sv} \cos^2 \alpha + \varepsilon_{Sh} \sin^2 \alpha$$

α is the polarization rotation angle between the PSR polarization basis and the natural polarization basis associated with the terrain.

The PSR provides direct measurements of horizontal emissivity ε_{Sh} and of vertical polarization emissivity ε_{Sv},.

PSR Data Gridding

- To facilitate further analysis and comparisons with *in situ* observations emissivity gridding onto a geographic 100-m resolution grid was applied.
- Small T_B offsets between adjacent gridded lines due to calibration drift were removed using the data from the line overlap area (~20% of the swath width).
- For grid cells with no corresponding radiometric footprints the algorithm interpolated the data using a weighted sphere-of-influence technique.
- Extrapolation outside the limits of the flight segment was not permitted.
- Thus, interpolation over small calibration gaps occurred but interpolation over larger gaps was precluded and the displayed data contains gaps.

Emissivity Images

- Small-scale variations within the given image map are related to the snowpack, land cover, surface temperature, and terrain elevation variations.
- Emissivity maps show detailed small-scale variations in the range of 0.75 — 1.0 for the low frequency channels, 0.5 — 1.0 range for the 37 GHz and 0.4 — 1.0 for the 89 GHz channels.
- Comparison of emissivity image maps with the land cover maps reveals that at each MSA pasture and row crop land show lower emissivity and forested areas showing increased emissivity.
- For a given channel and MSA the mean $\Delta\varepsilon$ between consecutive flights are in the 1 — 3% range for 6.9, 10.7, 18.7, and 37 GHz channels, as a result of fresh snowfall and surface temperature variations.

Emissivity Images: North Park

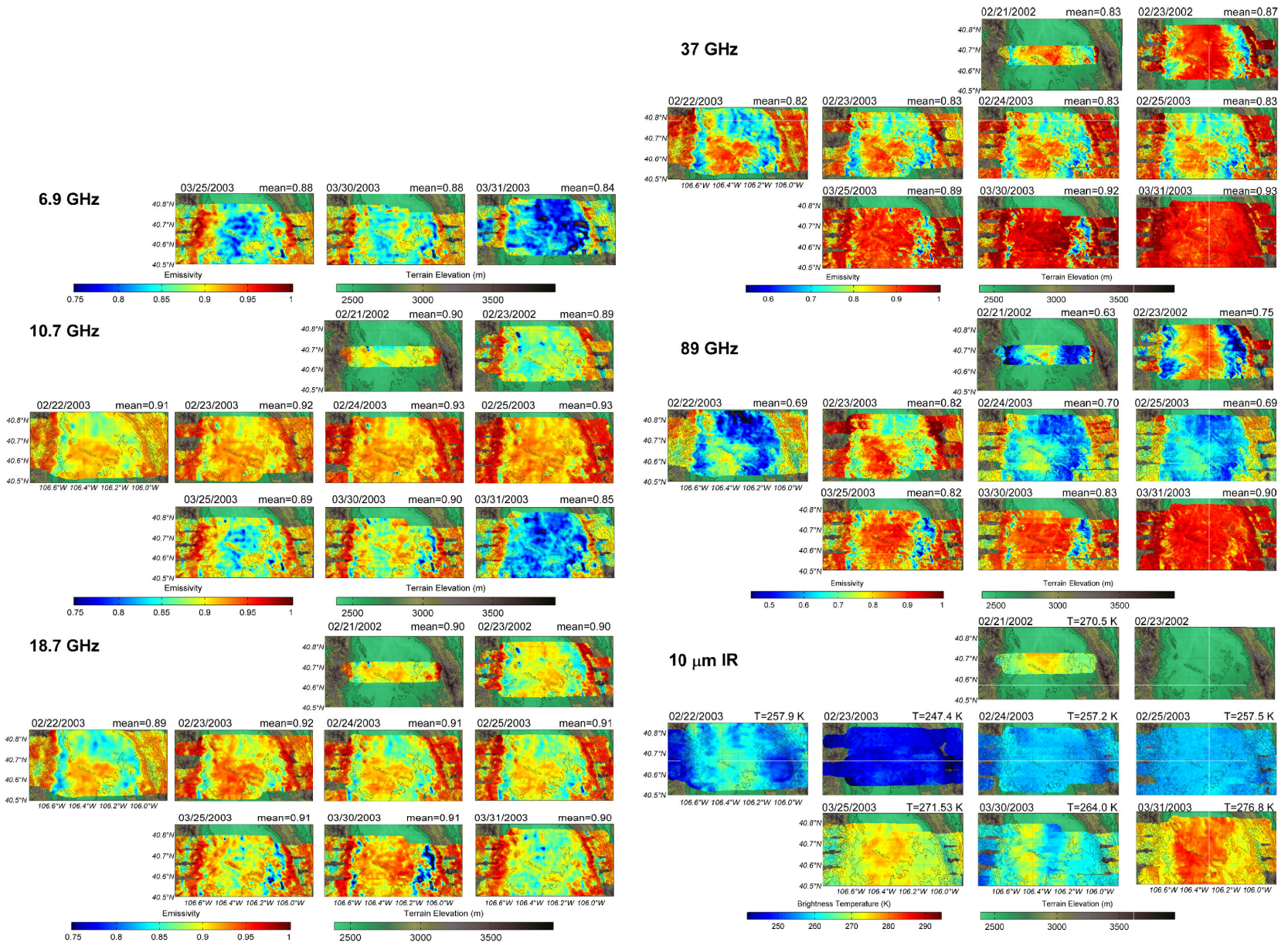

Emissivity Images: Rabbit Ears

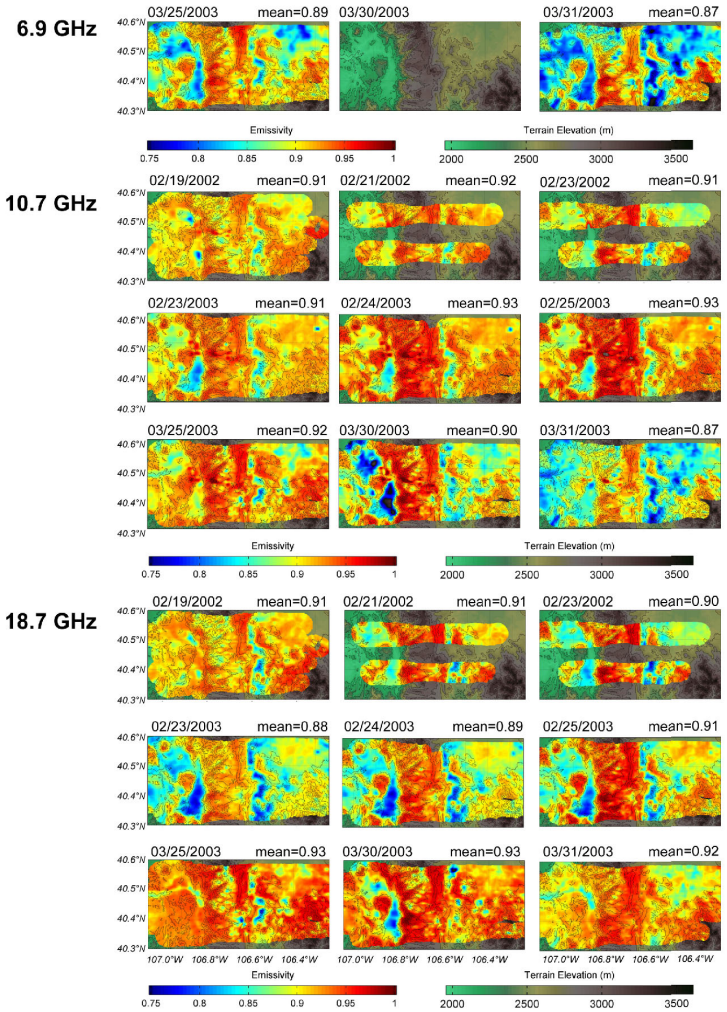

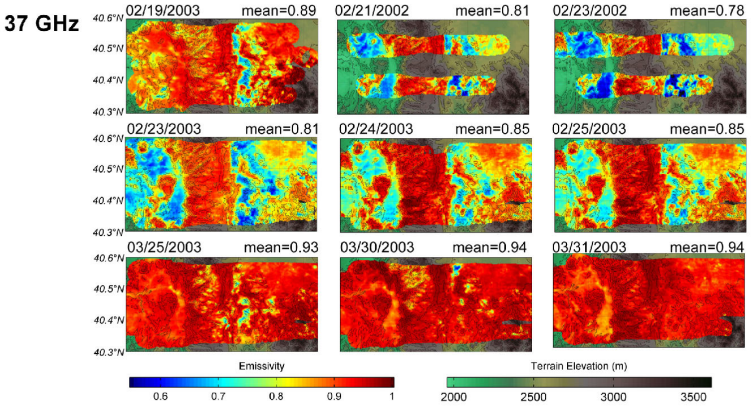

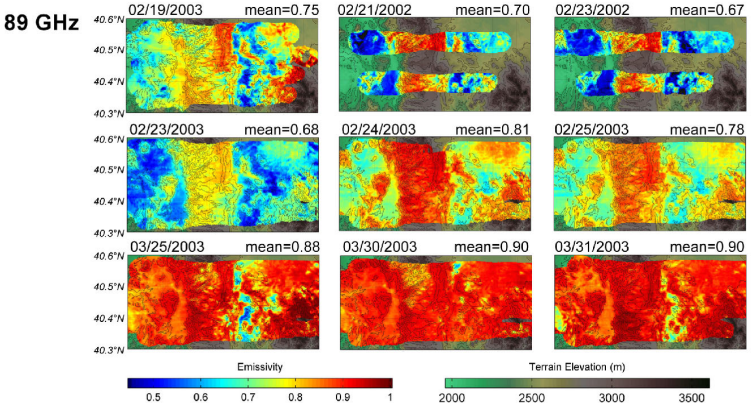

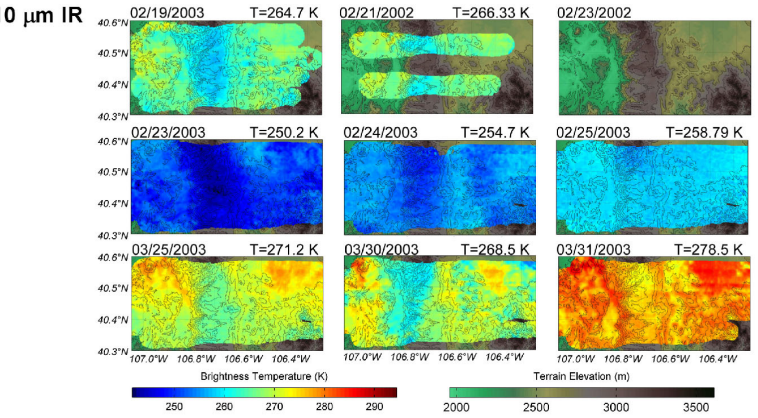

Emissivity Images: Fraser

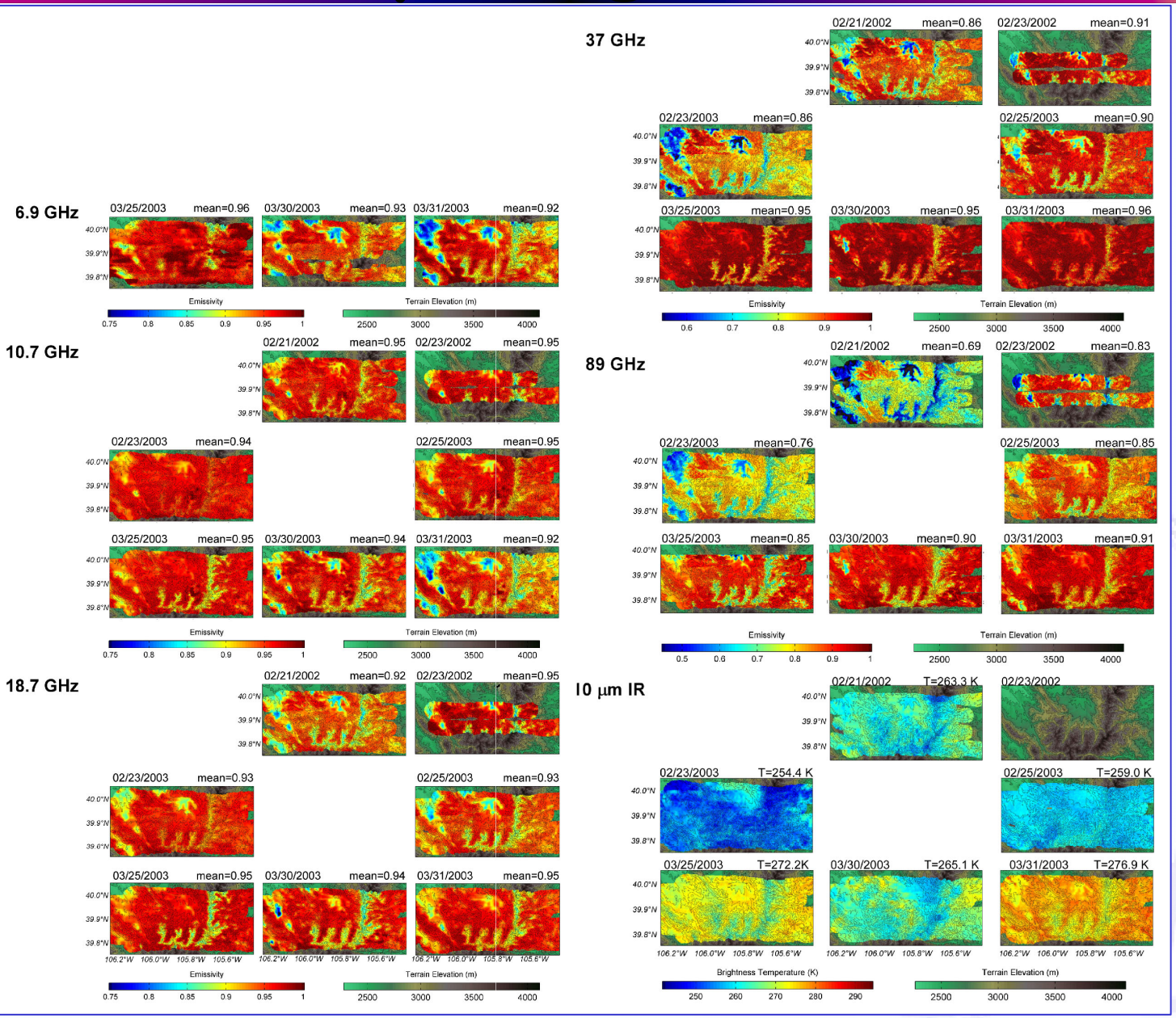

Emissivity Images

Two cases of anomalous behavior stand out:

- the February 2003 flights when the 89 GHz channel exhibited large variations on consecutive flight days due to the high sensitivity of 89 GHz channel to the snowpack state, and
- the 31 March, 2003 flights when the 6.9 GHz channel exhibited large drop in brightness temperature and 37 and 89 GHz channels exhibit a sharp increase due to snow melt and surface soil moisture increases.

89 GHz Channel Sensitivity to Precipitation

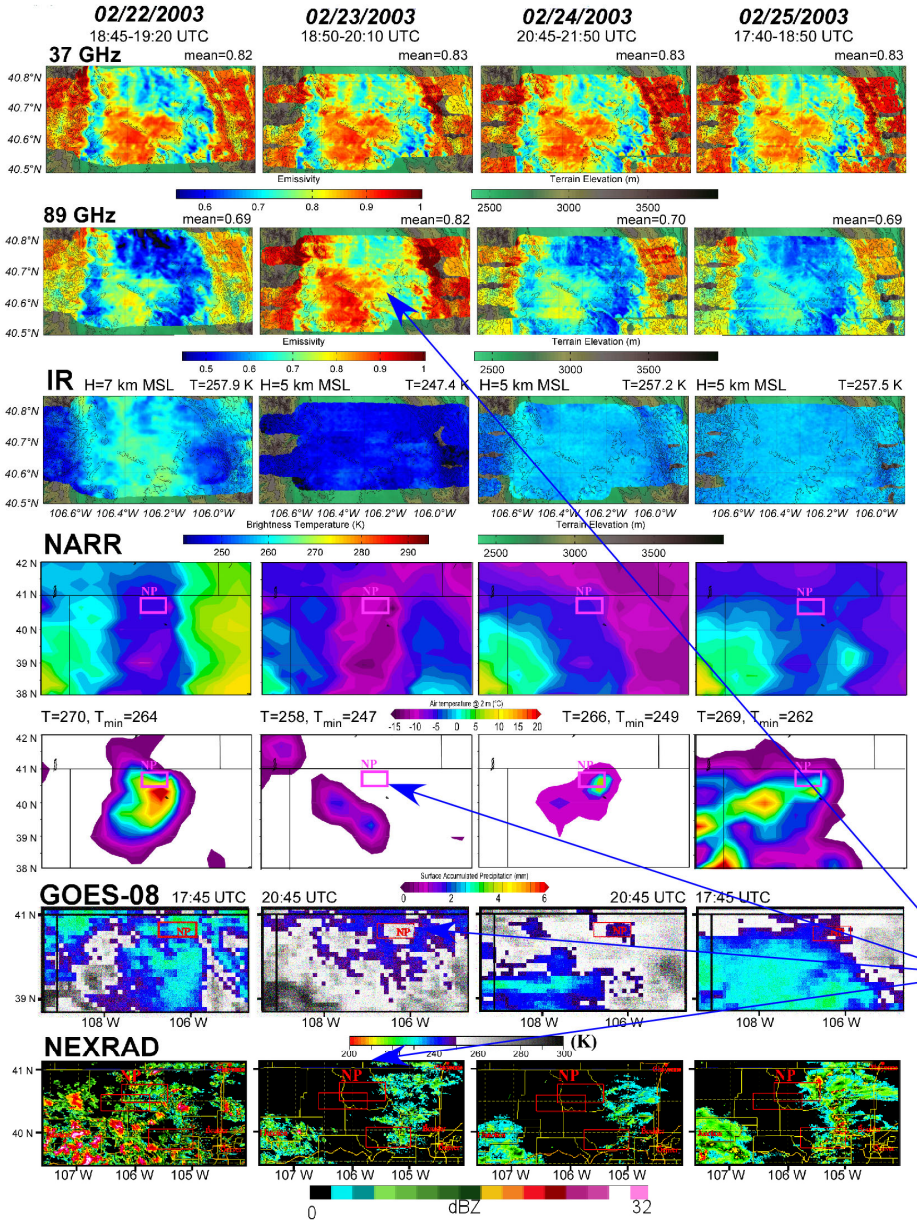

North Park MSA

MRT-modeling of 89GHz channelfor precipitation and cloud.

02/23/2003 RAOBT and Q profiles

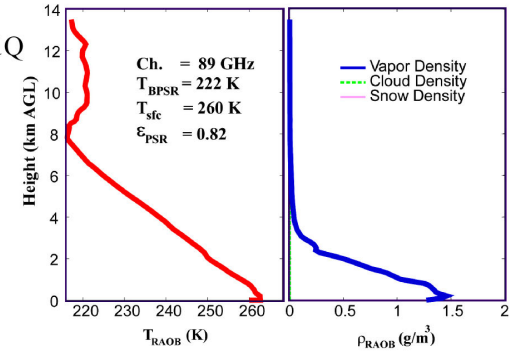

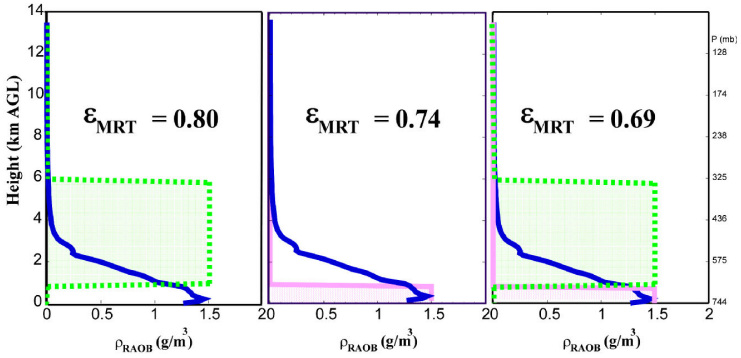

Previous day, 02/22/2003, GOES8-determined cloud and NEXRAD-determined precipitation

Mean ε_S on 02/23/2003 is 13% higher than on 02/22/2003 and 02/24/2003. We explain this by observing that NARR precipitation maps show no precipitation 02/23/2003

89 GHz Channel Sensitivity to Precipitation

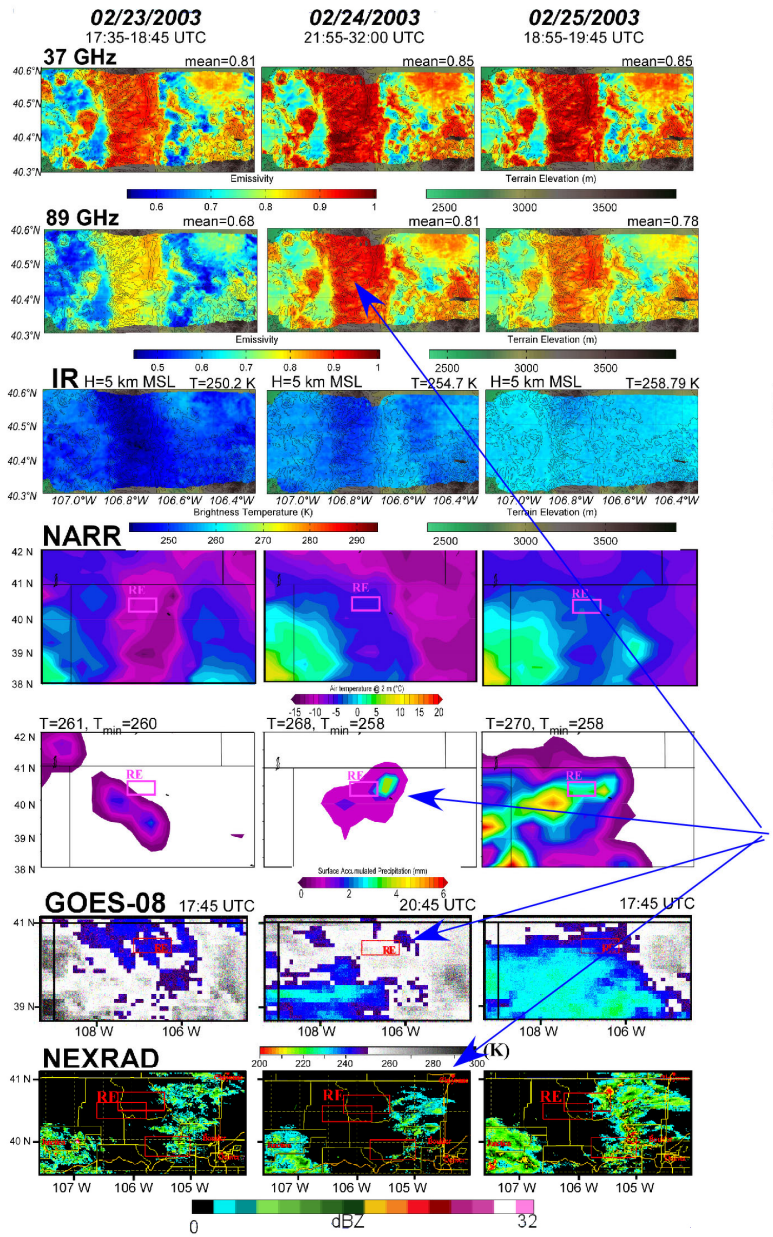

Rabbit Ears MSA

MRT-modeling of 89 GHz channel for precipitation and cloud

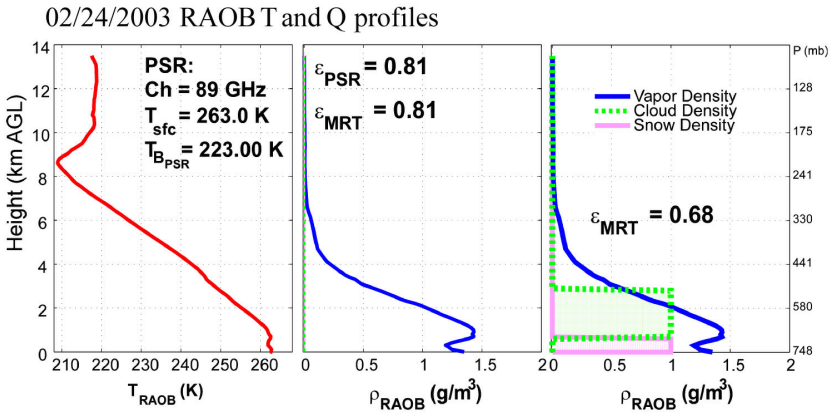

Previous day, 02/23/2003, GOES8-determined cloud and NEXRAD-determined precipitation

Mean ε_S on 02/24/2003 is 13% higher than on 02/23/2003. This is explained by observing that GOES8 shows clear over the MSA at that time, NEXRAD shows no precipitation and NARR precipitation maps shows very little precipitation accumulated during the previous 3-h.

89 GHz Channel Sensitivity to Precipitation

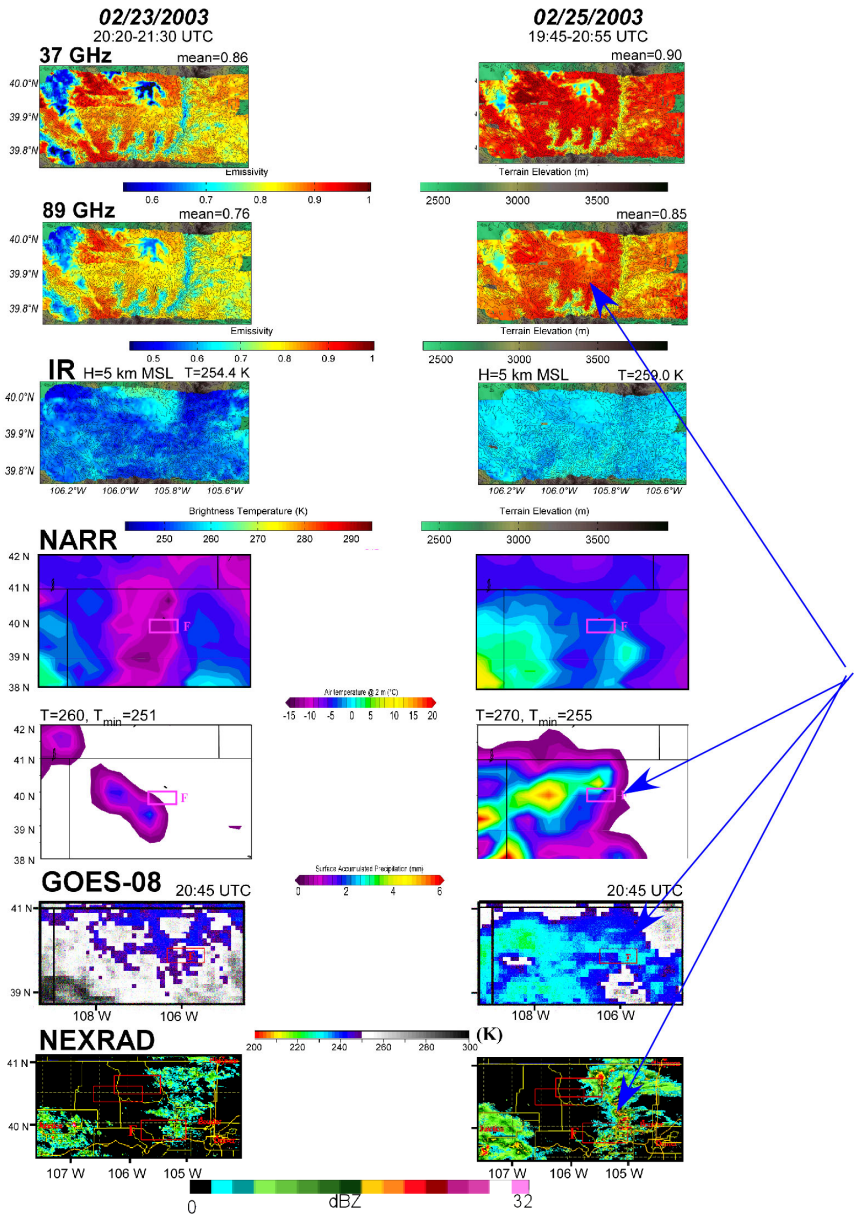

Fraser MSA

Mean ε_s on 02/25/2003 is 9% higher than on 02/23/2003. GOES8, NEXRAD, and NARR show cloud and precipitation on both days in varying degrees. However, surface air temperature is 10 degrees higher on the 02/25/2003.

Snowpack Classification*

Dry Winter Snow:

Snowpack consists of fresh snow that has not undergone any melting metamorphism.

Scattering is dominant as the frequency increases, and for frequencies smaller than ~9 GHz absorption is dominant.

Wet Snow:

Snowpack is a mixture of ice particles, water droplets, and air.

Even a very small amount of liquid water causes the snowpack to approach the non-reflecting condition of a blackbody.

At frequencies below ~ 9 GHz brightness temperatures are lower due to the water presence and at frequencies higher than ~21 GHz brightness temperatures are closer to the surface temperature.

Dry Re-Frozen Snow:

Snowpack with a firm top layer several centimeters thick.

The snow crystals become more spherical after melting and refreezing and the polarization difference drops.

* E. Schanda, C. Matzler, and K. Kunzi. "Microwave remote sensing of snow covers," *Int. J. Remote Sensing*, vol. 4, pp. 149–158, 1983.

Snowpack Classification

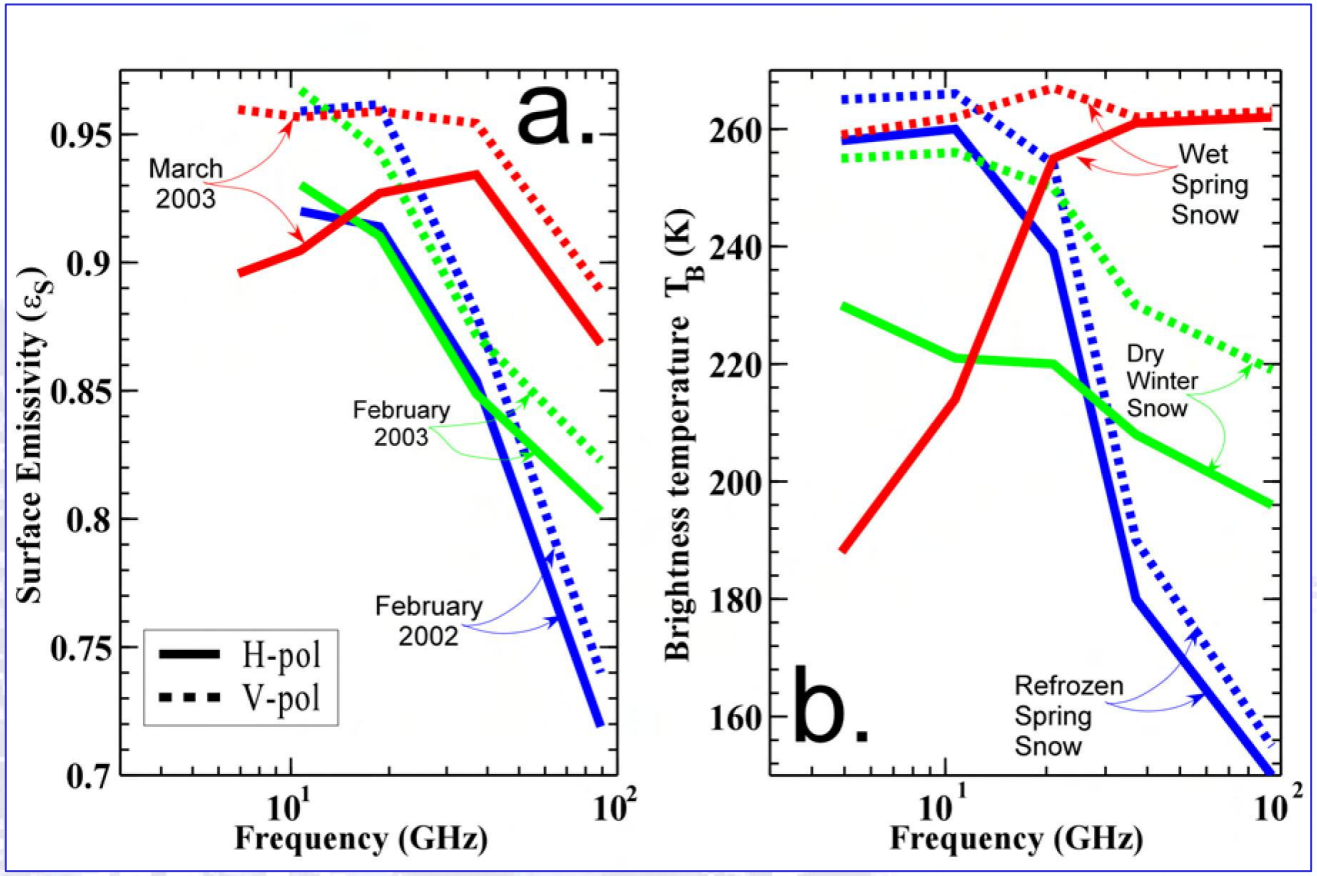

Spectral behavior of the average ε_S observed at H- & V-polarizations.

(a) Emissivity averaged over all extended MSAs for February 2002, February 2003, and March 2003.

(b) Spectral behavior of data collected in the Alpine regions and used for SWE classification as Dry Winter Snow, Refrozen Spring Snow, and Wet Spring Snow (Schanda et al., 1983, Figure 3).

Snowpack Classification

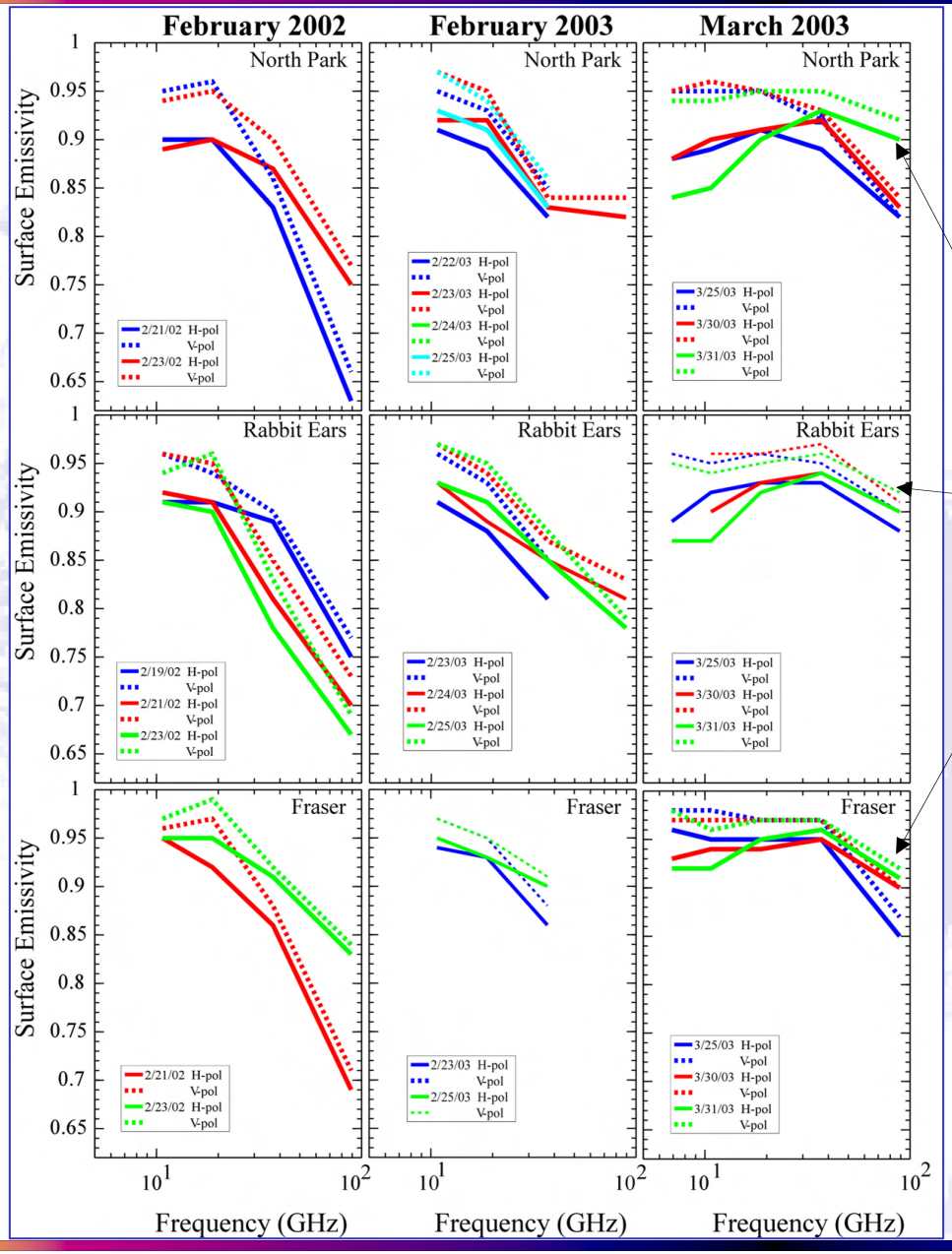

Spectral behavior of the average ε_S observed at H- & V-polarizations for each PSR observation day.

31 March indicates that the snow was wet.

Onset of Melting

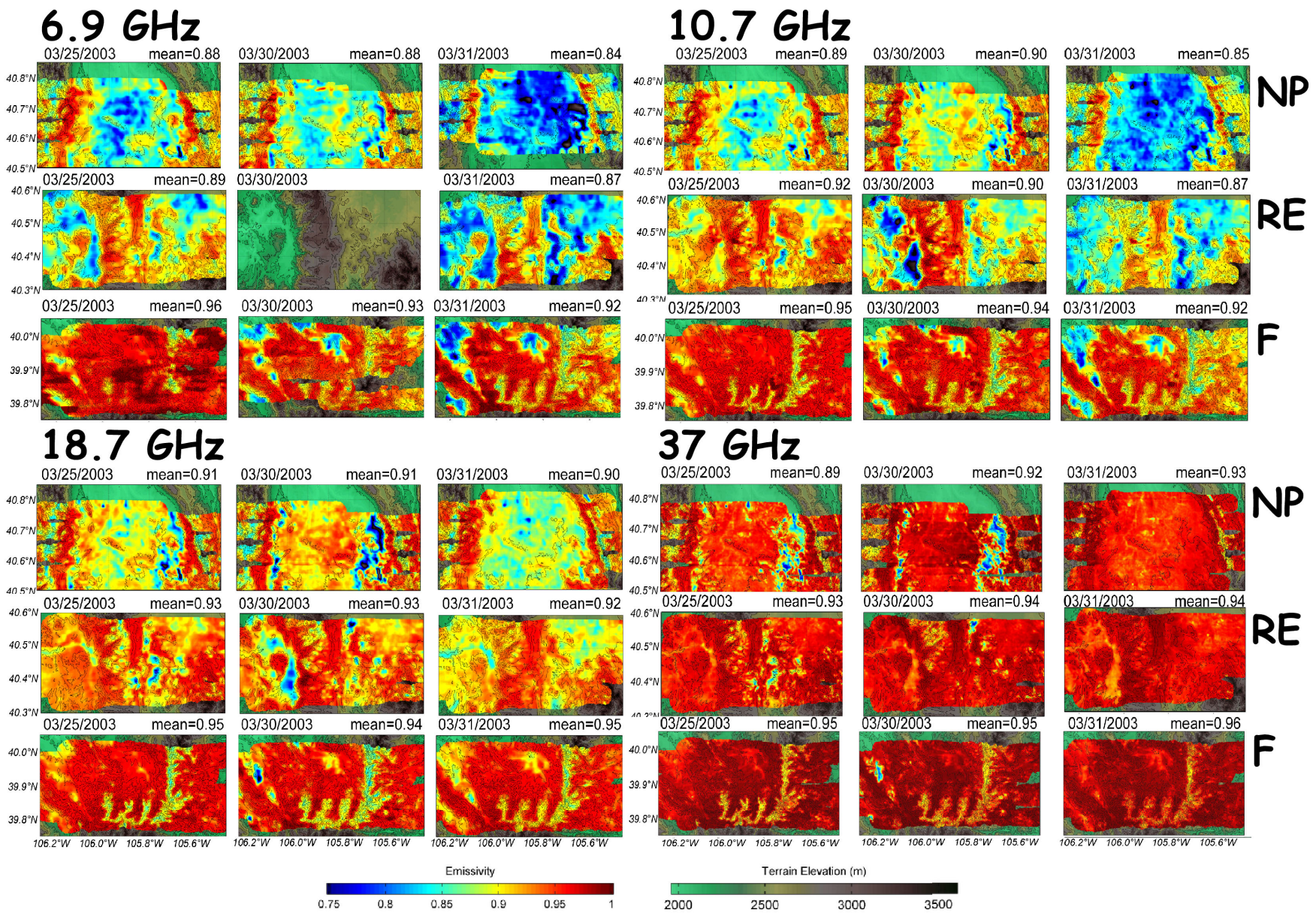

Validation

PSR SWE from Chang Formula

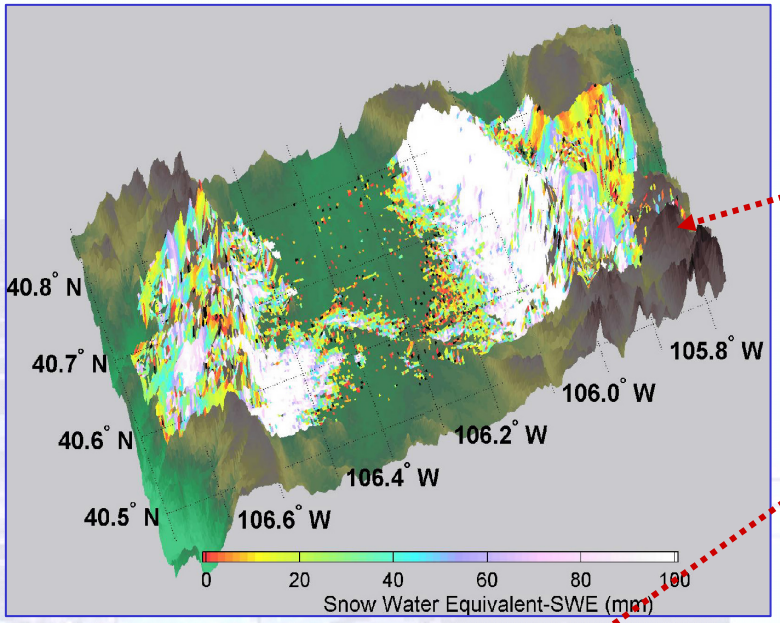

North Park

Rabbit Ears

Fraser

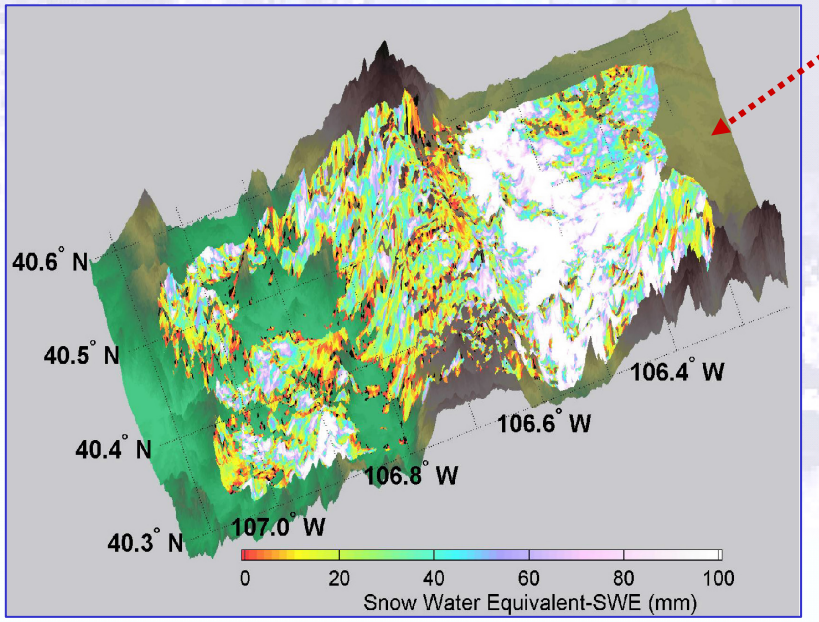

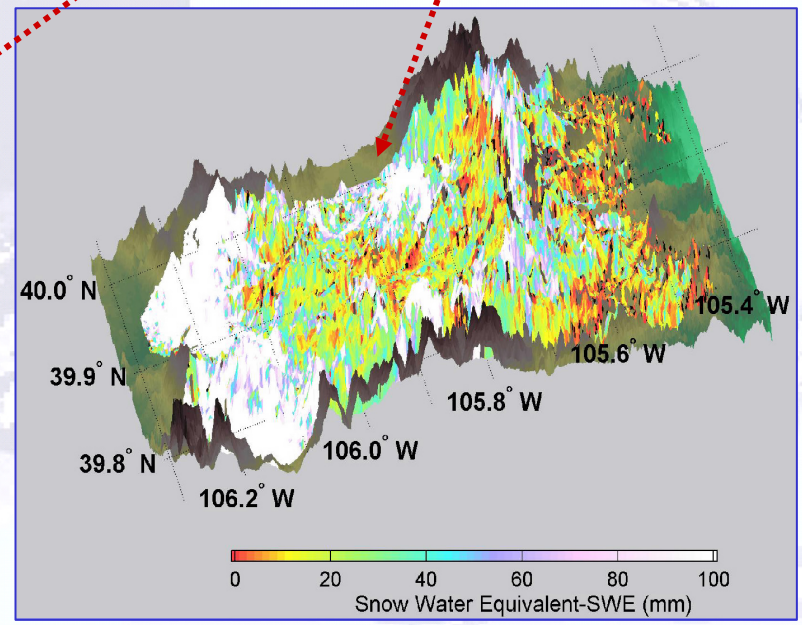

Validation Data Set

- The gridded-100 m resolution PSR microwave data set was used to estimate both T_B and ε_s at the locations of the ground-based *in situ* observations of SWE .
- All together, during the PSR flights there were 2707 data points, including 2107 from depth transects and 600 from snow pit observations. Of these, 403 were rejected as spurious or otherwise out of bounds, resulting in a final data set with 2304 points available for comparison.
- The 2304 data set of collocated PSR and ground-based measurements was comprised of 21 flights spanning two seasons that included drought, normal snowpack, and spring snowmelt. These data will be referred to as observed brightness temperatures, T_{Bobs}.

Ground Data Details

ISA Sample Locations

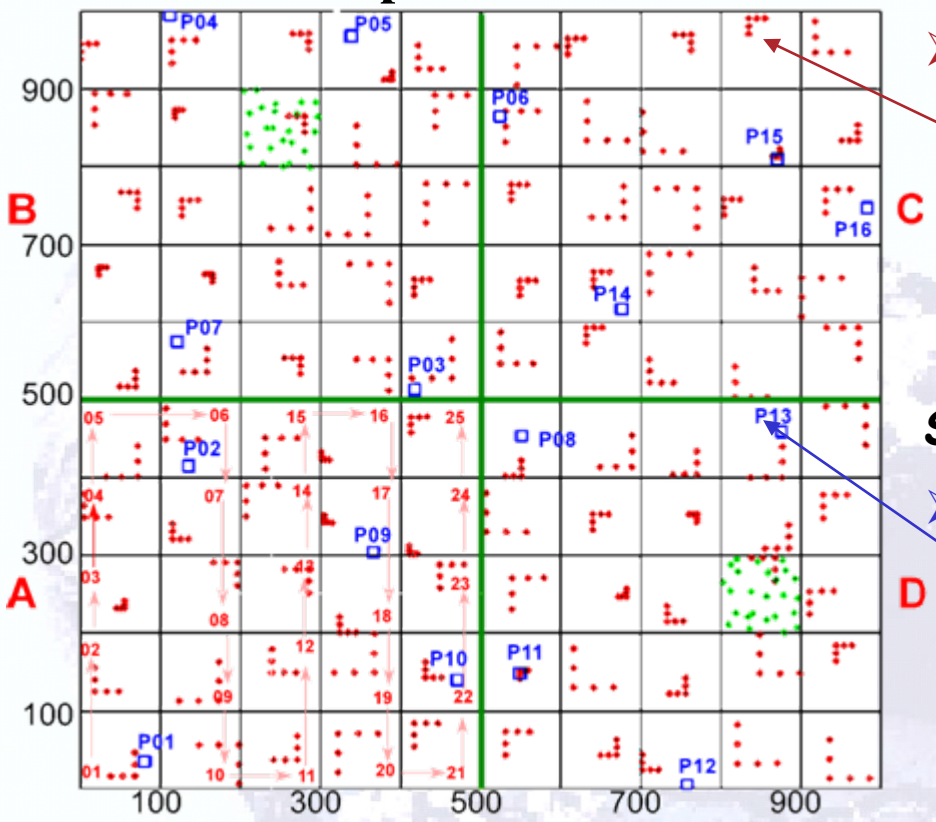

Transects measurements:

- Within each 100m x 100m grid cell, snow depth, surface wetness, snow temperature, soil temperature, and canopy cover were observed at points along transects with randomly selected origin, interval, and orientation.

Snow Pit measurements:

- In four randomly located snow pits within each 500m x 500m grid cell, vertical profiles of density, temperature, stratigraphy and grain size were measured in addition to snow depth, surface wetness, and canopy cover.

- SWE for each transect was calculated using the mean snow depth from the multiple transect points and the mean snow density observed at the nearest snow pit.
- Similarly each transect was assigned the grain size values from the nearest snow pit.

HUT Modeling

- To complement the PSR data set, we used Helsinki University of Technology (HUT) model to obtain T_B for each collocated airborne/*in situ* record.
- HUT snow emission model describes emission behavior of a homogeneous snowpack as function of SWE, effective grain size, and density of snow.
- Hut also uses semi-empirical parameterizations of forest canopy, atmospheric optical thickness, soil roughness, and it includes the effects of the layer boundaries.
- These data will be referred to as modeled brightness temperatures, T_{mod}.

PSR Image Data Examples

The PSR image data generally exhibit the expected frequency dependence, with significantly lower T_{Bobs} at 37 GHz and 89 GHz than observed for 21.5 GHz.

North Park

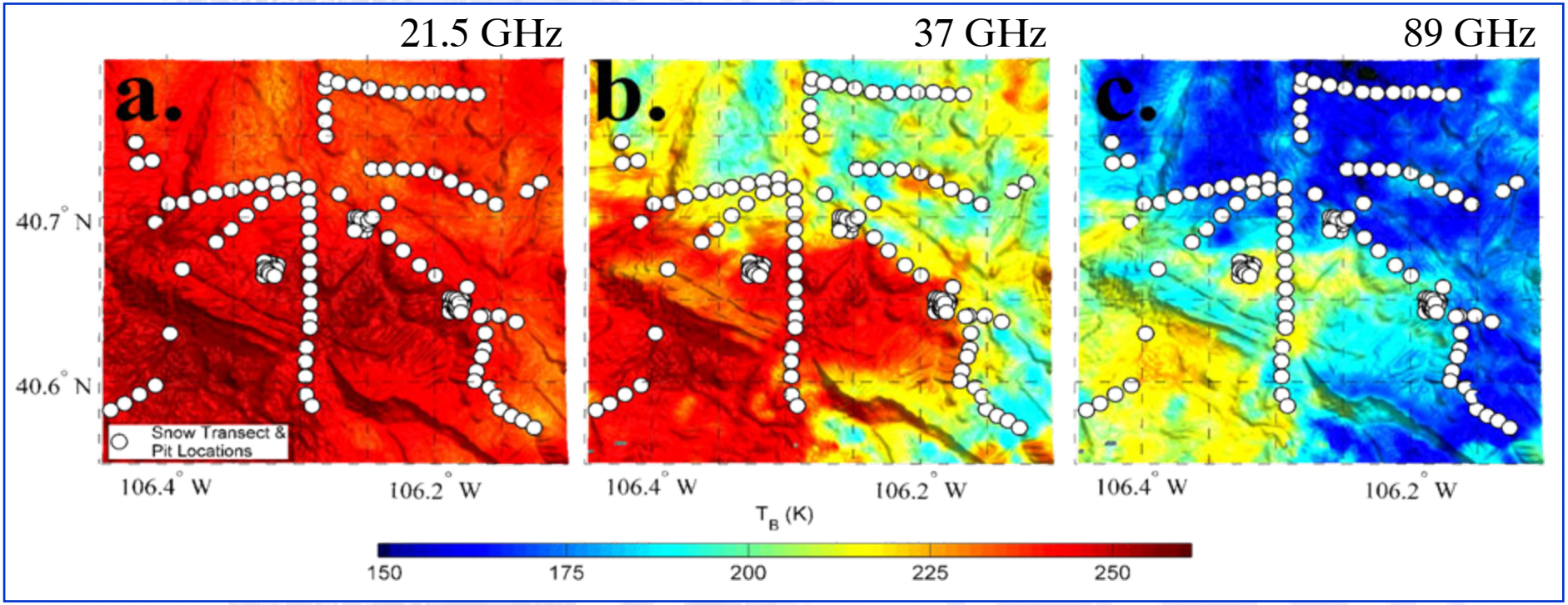

PSR Image Data Examples

Rabbit Ears

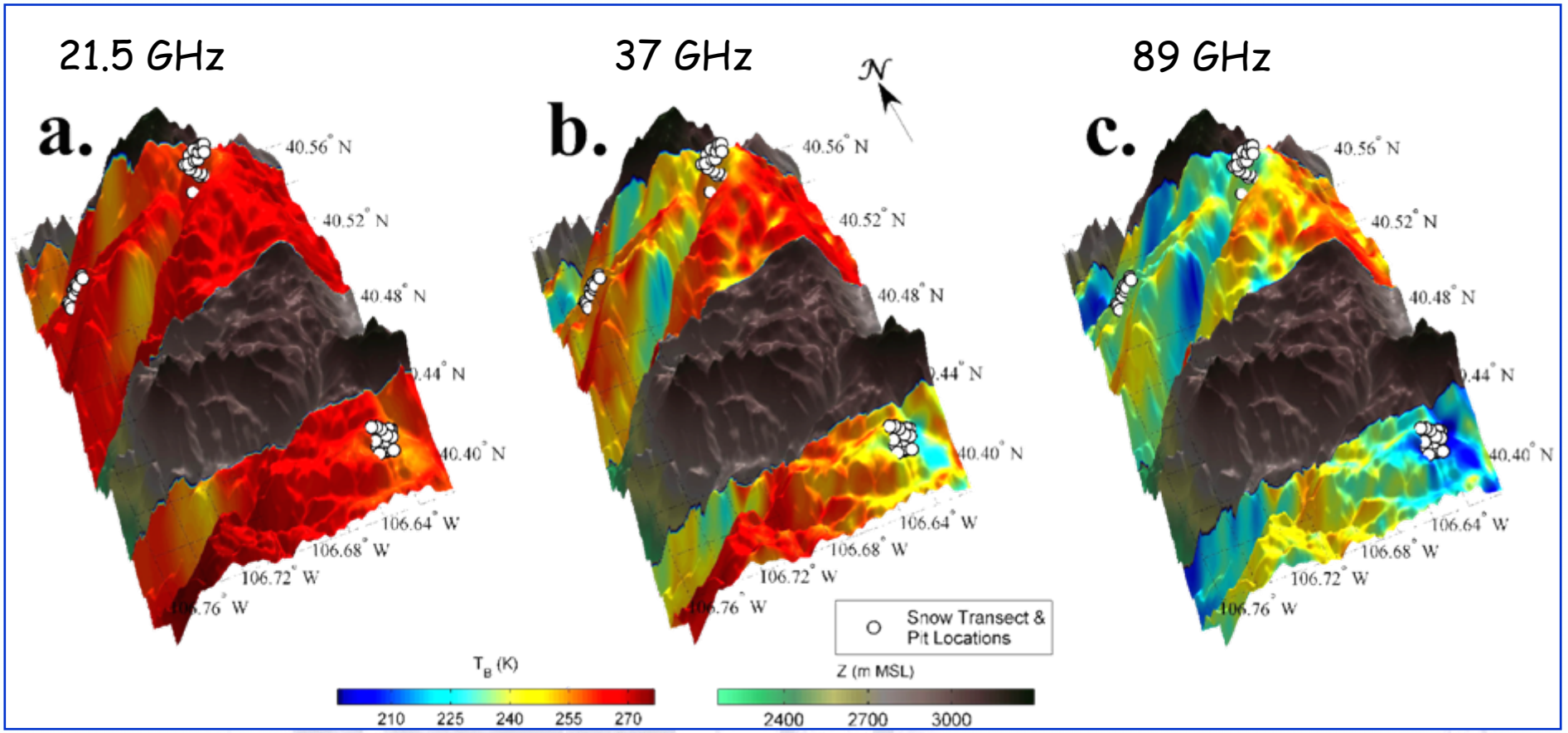

PSR Image Data Examples

Fraser

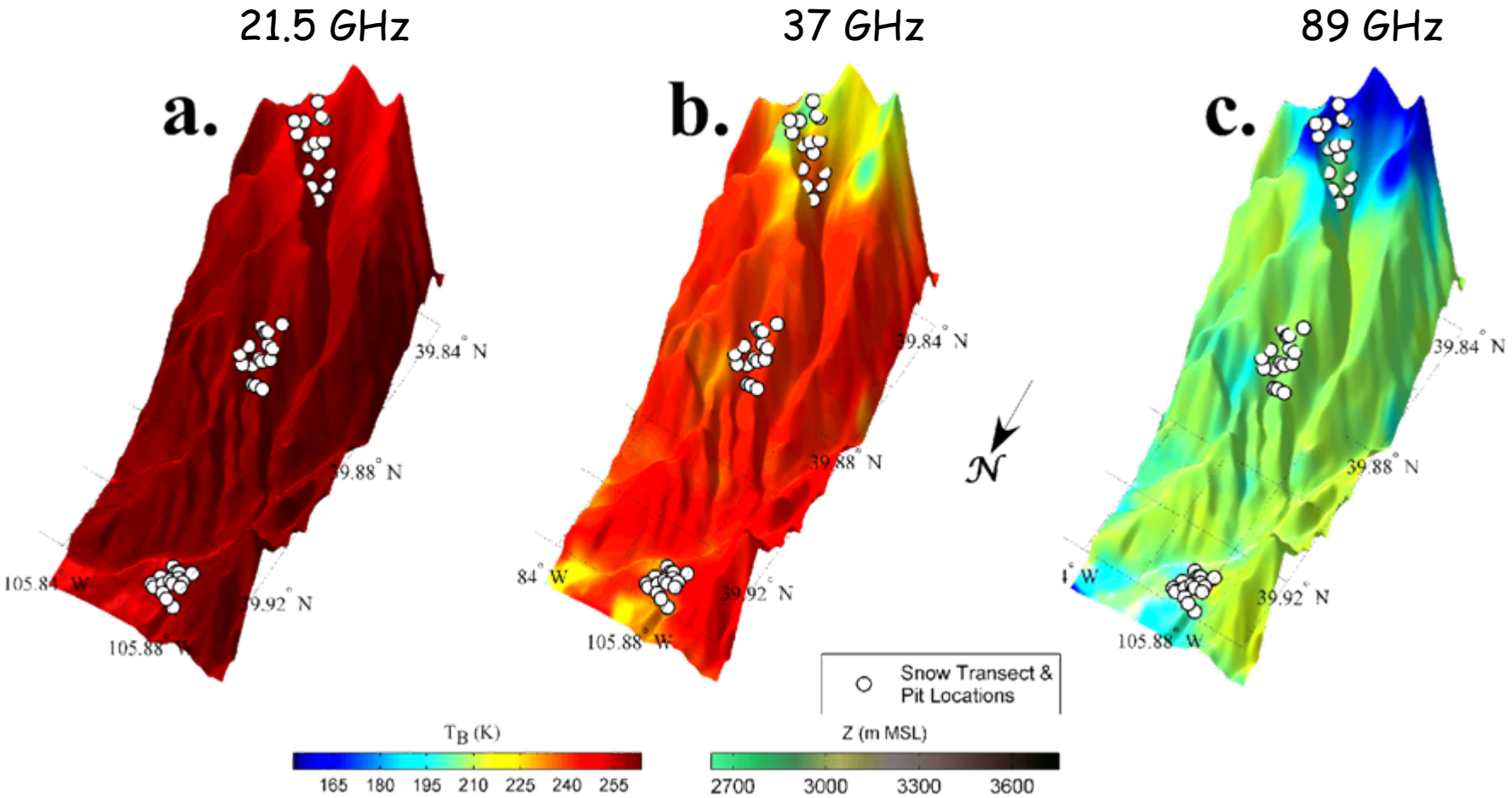

Collocated Data Frequency Dependence on SWE

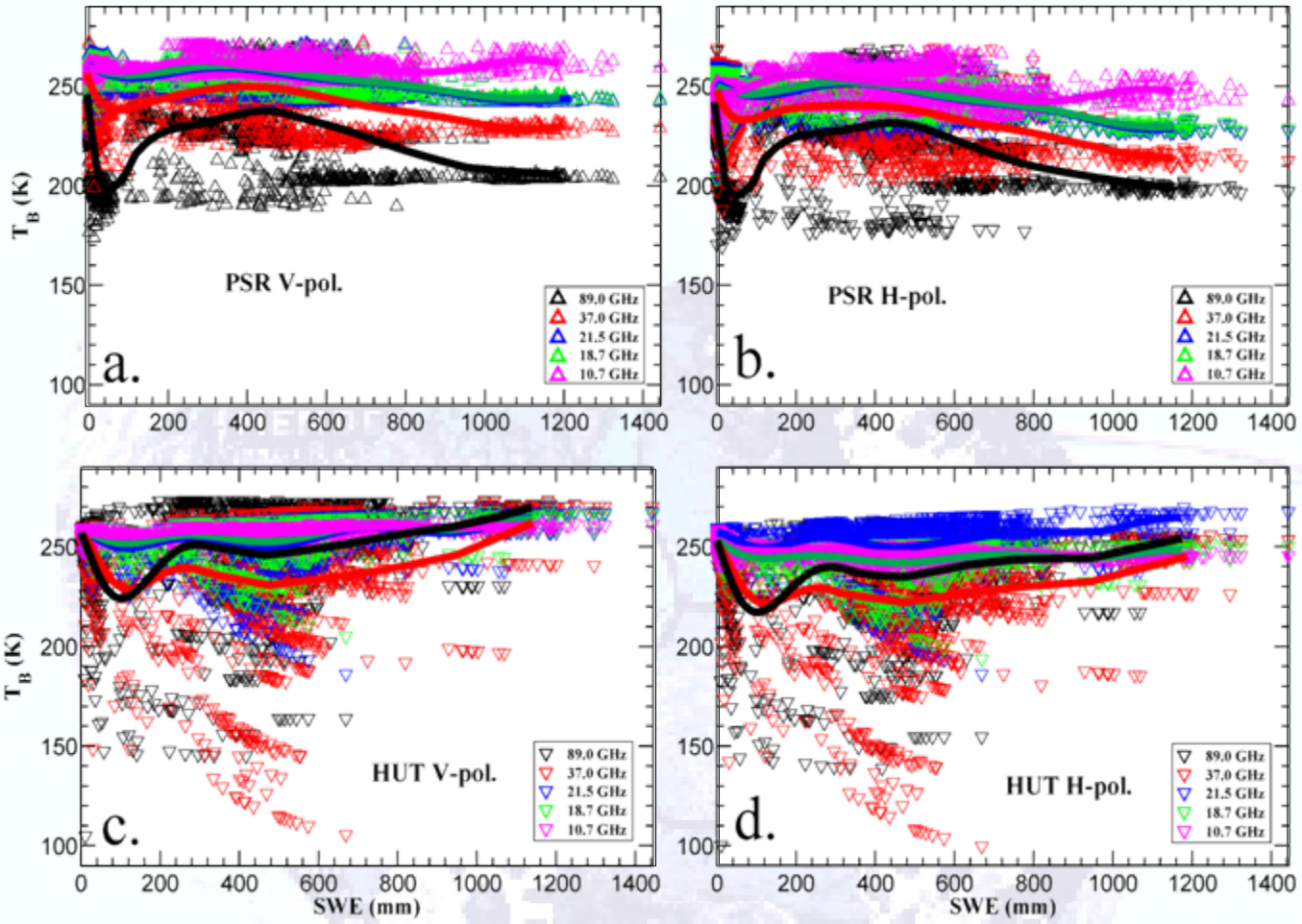

- T_{Bobs} and T_{Bmod} response to SWE for the entire 2304-point dataset generally fall within the same range.
- The data extend from SWE=0 to SWE=1445 mm and cover a wide range of ground, snow and weather conditions.
- A 10-degree polynomial fitted curves for 37 and 89 GHz channels show a quick drop in T_B up to 80-mm SWE, then change direction and exhibit an upward trend with increasing SWE.
- Lower frequencies show a similar but much less pronounced response. The 10.7, 18.7, and 21.5 GHz fitted curves frequently overlap.

- These patterns are consistent with historical datasets Matzler 1982, and Schanda et al. 1983, where it has been suggested that the reversal of the T_B versus SWE slope may be due to a prevalence of larger snow grains in shallow snowpacks.

Collocated Data T_B Spectral Dependence

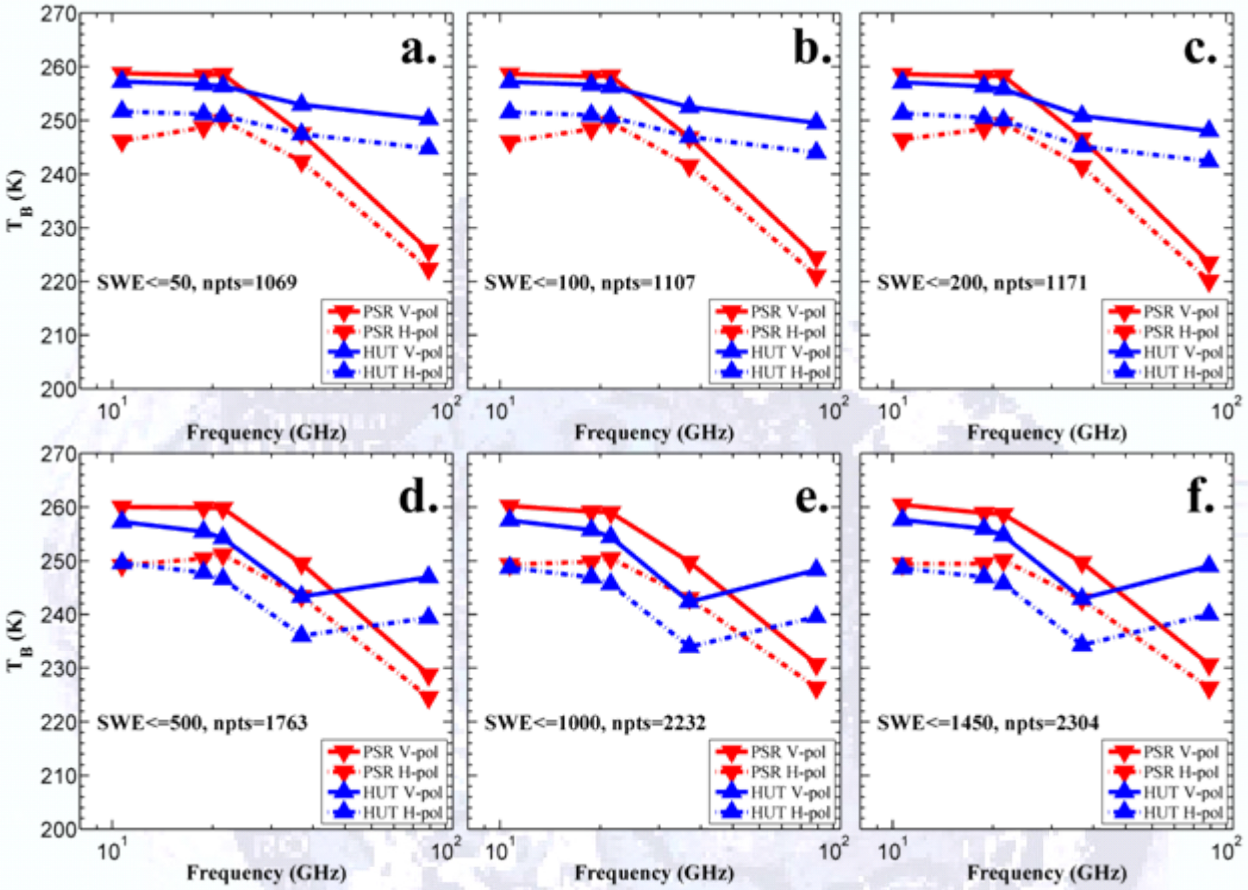

- Observed PSR spectra exhibit characteristics of the refrozen snow for all magnitudes of SWE. T_{Bobs} drops sharply with increasing frequency and the polarization difference ($\Delta T_B = T_{BV} - T_{BH}$) is small.

- Modeled spectra suggest the presence of wet snow when SWE > 200 mm is included. T_{Bmod} decreases across all frequencies for SWE <= 200 mm, but increases at 89 GHz with greater SWE. This suggests that at this level of SWE in the HUT-model the snowpack behaved as wet spring snow.

Collocated Data Response to Grain Size

The lengths of the major and minor axes of multiple representative small, medium, and large, snow grains within each major stratigraphic layer were measured.

Thus, there were nine grain size cathegories observed, i.e. minimum, average, and maximum, of the small, medium, and large.

T_{Bobs} and T_{Bmod} were plotted against observed SWE for each of the nine observed grain size categories and for all PSR channels and revealed that:

- at 89 GHz, T_{Bmod} most closely matched T_{Bobs} for the small minimum grain size,
- at lower frequencies T_{Bmod} most closely matched T_{Bobs} for the medium minimum grain size.

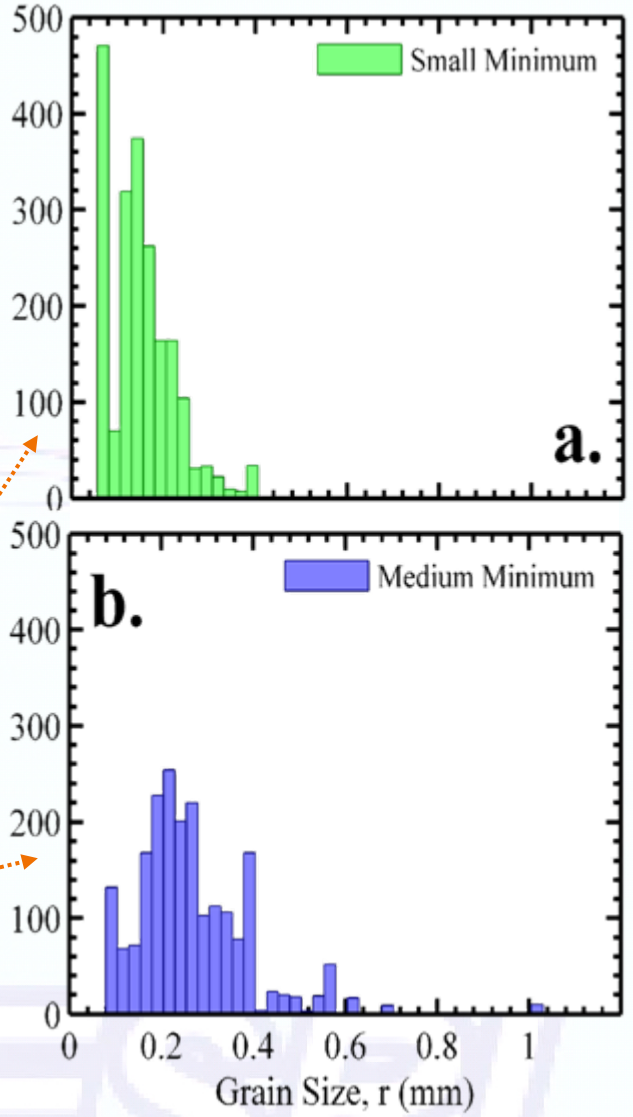

Vegetation- and Wetness-filtered Data

To create a dry snow subset with uniform characteristics the following filters were used:

- All points with any type of macro-vegetation present were removed, reducing the data set to 1179 points.
- All points with *in situ*-observed wet or moist snow were removed, reducing the dataset further to 601 points.
- The third filter required that the maximum snow pit and the surface temperature remain below freezing, reducing the data set finally to 224 points.

Vegetation- and Wetness-filtered Data

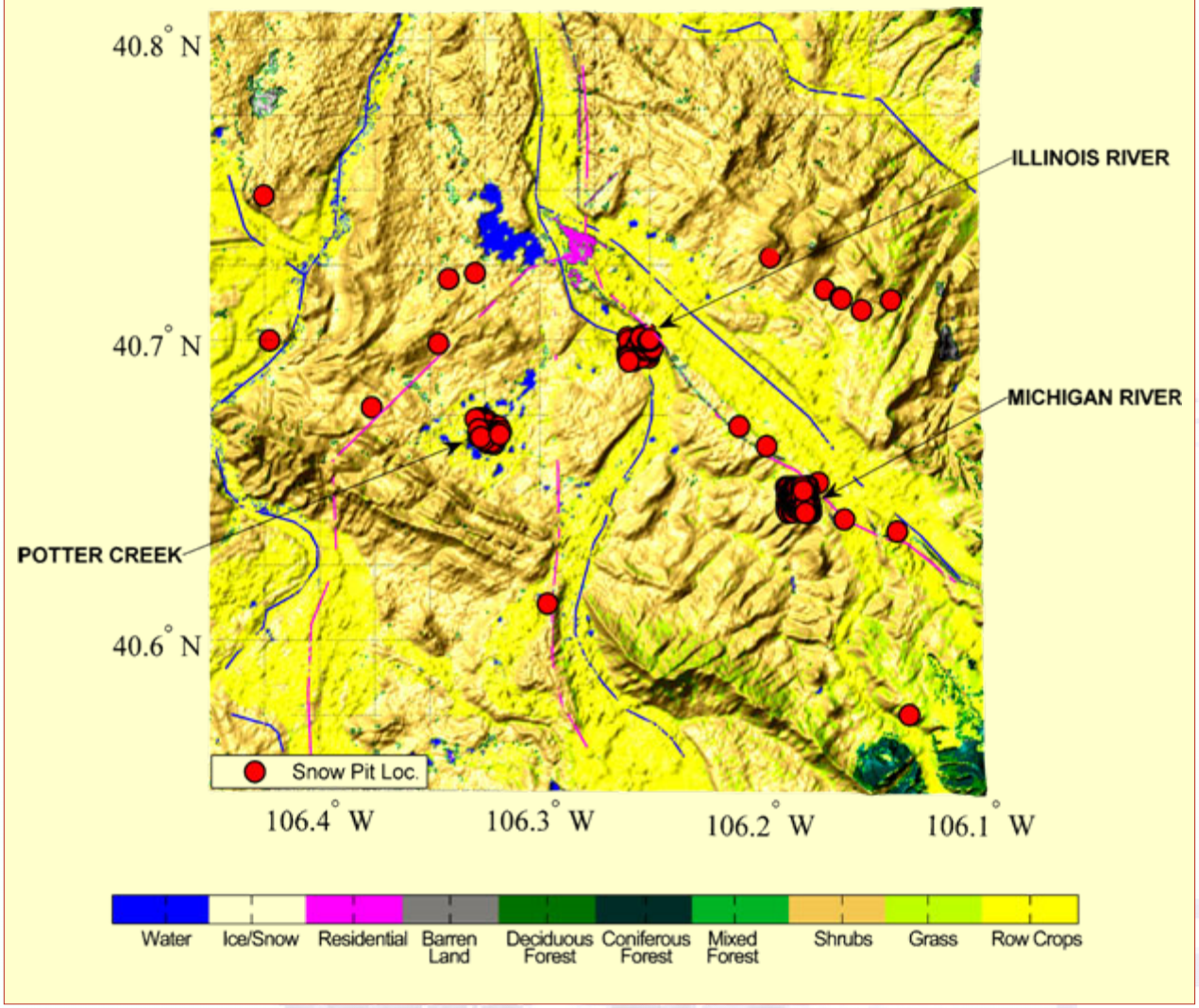

After filtering:

- The maximum SWE value in the data set dropped from 1445 mm to 95 mm.
- All remaining points after filtering were located in the North Park MSA.

Filtered Data Frequency Dependence on SWE

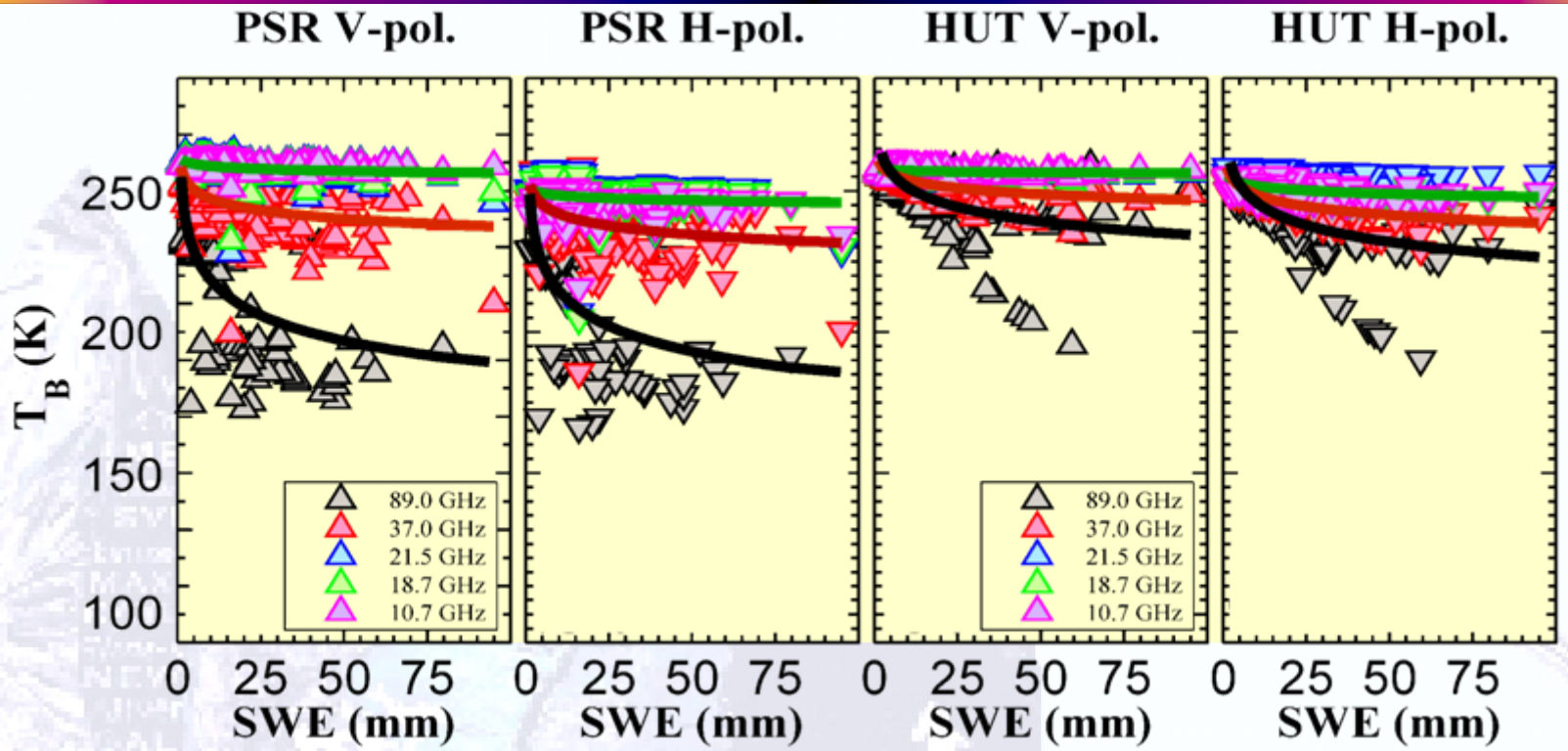

- For each frequency a curve of the form $y(x)=Cx^n$ was fitted to the filtered data which exhibited much less scatter.
- A minor drop in T_B with increasing SWE is evident in the 10.7, 18.7, and 21.5 GHz where the fitted curves overlap each other.
- However, in the 37 and 89 GHz data a large initial drop with increasing SWE with a subsequent leveling off is shown in both PSR and HUT data for both polarizations.
- The filtered data and fitted curves closely resemble the theoretical curves in Chang 1986.

Filtered Data Characteristics

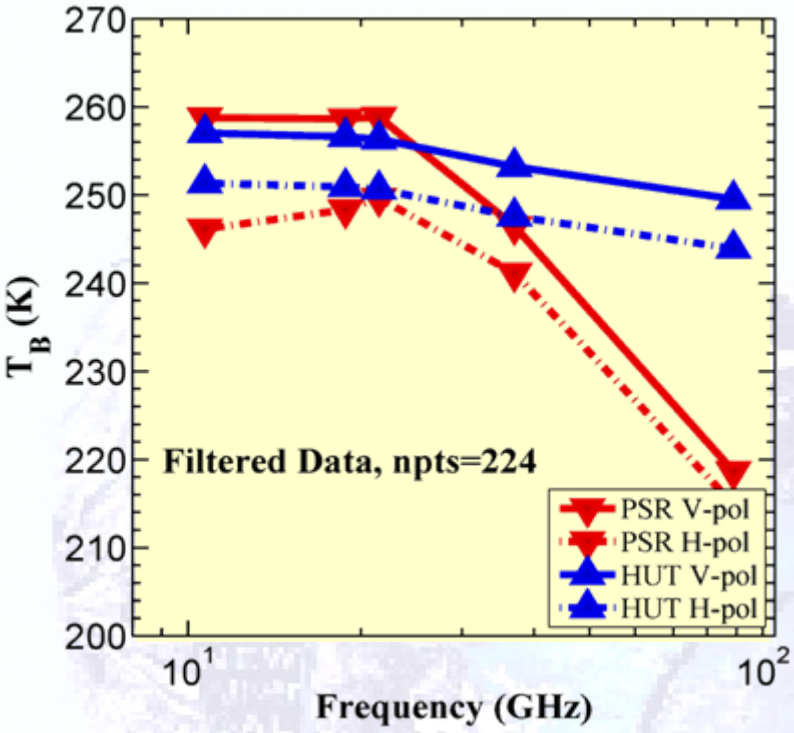

- T_{Bobs} and T_{Bmod} spectra for the filtered dataset exhibit characteristics of refrozen snow (Schanda et al. 1983).
- T_B drops with increasing frequency and the polarization difference ($\Delta T_B = T_{BV} - T_{BH}$) is small.

- Histograms of the small minimum and medium minimum grain size in the filtered dataset show variation from 0.1 mm to 0.4 mm.

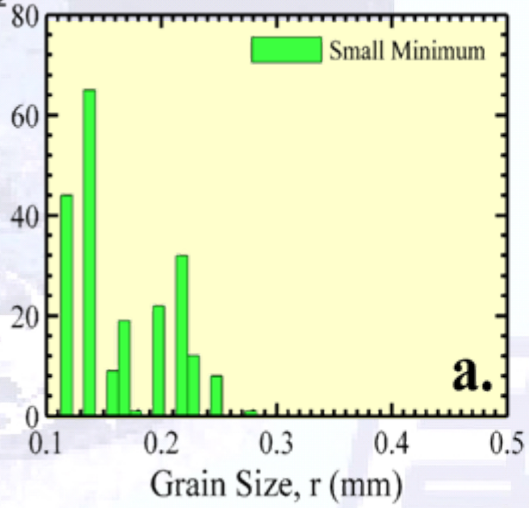

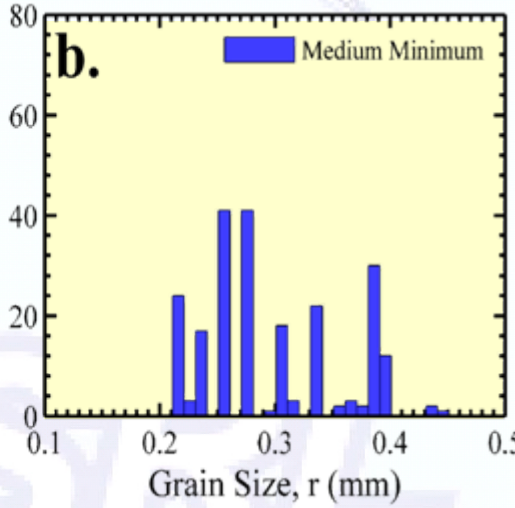

Regression Analysis for Filtered Data

- Using the filtered data set, relationships between SWE and all T_B two-frequency difference combinations (f_{lower} - f_{higher}) were analyzed.
- The best-fit regression line in the form of $y=A0+A1 \cdot SWE$, where A0 varies with T_B function and the snow conditions, and A1 gives the microwave response to SWE was estimated.
- The correlation coefficient (R) and the RMS values of the regression were computed and compared with the results for the SMMR data from Finland, Hallikainen, M. T. and P. A. Jolma 1992.

Regression Analysis for Filtered Data

	PSR			HUT			Hallikainen: South (forest)			Hallikainen: North		
	A1	R	rms	A1	R	rms	A1	R	rms	A1	R	rms
10.7H	-0.016	-0.100	2.88	-0.087	-0.533	2.31	0.012	0.040	6.30	-0.048	-0.210	3.40
10.7V	-0.026	-0.361	1.05	-0.021	-0.279	1.13	0.038	0.160	3.80	-0.005	-0.120	2.10
18.7H	-0.072	-0.330	3.29	-0.107	-0.616	2.23	-0.048	-0.130	8.10	-0.113	-0.430	4.90
18.7V	-0.059	-0.438	1.95	-0.037	-0.432	1.24	-0.002	-0.010	4.90	-0.041	-0.190	3.00
21.5H	-0.088	-0.370	3.52	-0.118	-0.651	2.20	-0.027	-0.020	16.20	-0.177	-0.100	14.90
21.5V	-0.083	-0.476	2.47	-0.048	-0.497	1.34	0.040	0.030	12.70	-0.052	-0.060	14.70
37.0H	-0.258	-0.508	6.99	-0.239	-0.788	2.98	-0.159	-0.300	10.10	-0.300	-0.540	8.20
37.0V	-0.248	-0.538	6.22	-0.172	-0.658	3.14	-0.123	-0.330	6.80	-0.226	-0.550	5.90
89.0H	-0.934	-0.659	14.52	-0.424	-0.604	8.93						
89.0V	-0.945	-0.661	14.54	-0.487	-0.678	8.43						
10.7H-37H	0.242	0.509	6.55	0.148	0.653	2.74						
10.7V-37V	0.218	0.550	5.33	0.151	0.655	2.78	0.162	0.490	5.20	0.233	0.630	5.10
10.7V-37H	0.233	0.511	6.26	0.218	0.807	2.55	0.199	0.420	8.40	0.310	0.590	7.40
18.7H-37H	0.186	0.535	4.70	0.131	0.662	2.38	0.113	0.450	4.00	0.193	0.570	4.90
18.7V-37V	0.189	0.555	4.52	0.134	0.665	2.42	0.124	0.560	3.40	0.187	0.620	4.30
18.7V-37H	0.199	0.515	5.29	0.202	0.814	2.30	0.162	0.450	6.30	0.260	0.590	6.40
21.5H-37H	0.165	0.538	4.27	0.121	0.665	2.16						
21.5V-37V	0.169	0.546	4.03	0.123	0.668	2.20	0.110	0.470	3.90	0.159	0.560	4.10
21.5V-37H	0.175	0.501	4.82	0.191	0.816	2.16	0.148	0.400	6.60	0.237	0.570	6.10
Func 1	0.189	0.551	4.54	0.133	0.663	2.40	0.119	0.530	3.40	0.191	0.610	4.50
10.7H-89H	0.948	0.662	14.47	0.396	0.597	8.49						
10.7V-89V	0.891	0.659	13.71	0.403	0.596	8.69						
18.7H-89H	0.839	0.664	12.75	0.379	0.595	8.20						
18.7V-89V	0.853	0.658	13.14	0.386	0.593	8.38						
21.5H-89H	0.817	0.663	12.43	0.368	0.592	8.02						
21.5V-89V	0.821	0.655	12.78	0.375	0.590	8.21						
37H-89H	0.566	0.662	8.63	0.248	0.525	6.42						
37V-89V	0.599	0.661	9.16	0.252	0.522	6.58						
Func1=0.5(18H-37H+18V-37V)												

	PSR	HUT	HS	HN
A1	**0.19**	**0.15**	**0.14**	**0.22**
R	**0.54**	**0.71**	**0.47**	**0.59**
RMS	**4.86**	**2.41**	**5.15**	**5.35**

Averaged 37 GHz ΔT_B

Retrieval Algorithm

Correlation Analysis for the Filtered Data Set

- Randomly selected half of the points in the filtered data set were used in the ordinary least-square multiple linear regression algorithm to fit SWE as a function of the T_B differences (ΔT_B) and return a vector of regression coefficients for two different cases:

  a) 10.7, 18.7, and 21.5 GHz channels and 37 GHz channel,

  b) 10.7, 18.7, and 21.5 GHz channels and 37 GHz together with ΔT_B between 10.7, 18.7, 21.5, and 37 GHz channels and 89 GHz channel

- The remaining half of the filtered dataset was used to compute SWE from the microwave observations and compare computed SWE with the observed SWE.

Correlation Analysis for the Filtered Data Set

Multiple regression fit involving ΔT_B with only 37 GHz :

$$SWE_{calc} = 15.1 - 3.9(T_{B10V} - T_{B37V}) + 17.8(T_{B18V} - T_{B37V}) - 14.9(T_{B21V} - T_{B37V} + 1.0(T_{B10H} - T_{B37H}) - 6.0(T_{B18H} - T_{B37H}) + 6.52(T_{B21H} - T_{B37H})$$

Multiple regression fit involving both 37 GHz and 89 GHz ΔT_B :

$$SWE_{calc} = 26.9 - 5.0(T_{B10V} - T_{B37V}) + 34.3(T_{B18V} - T_{B37V}) - 27.5(T_{B21V} - T_{B37V}) + 1.6(T_{B10H} - T_{B37H}) - 9.1(T_{B18H} - T_{B37H}) + 6.0(T_{B21H} - T_{B37H}) - 2.4(T_{B10V} - T_{B89V}) - 2.2(T_{B18H} - T_{B89H})$$

Correlation Analysis for the Filtered Data Set

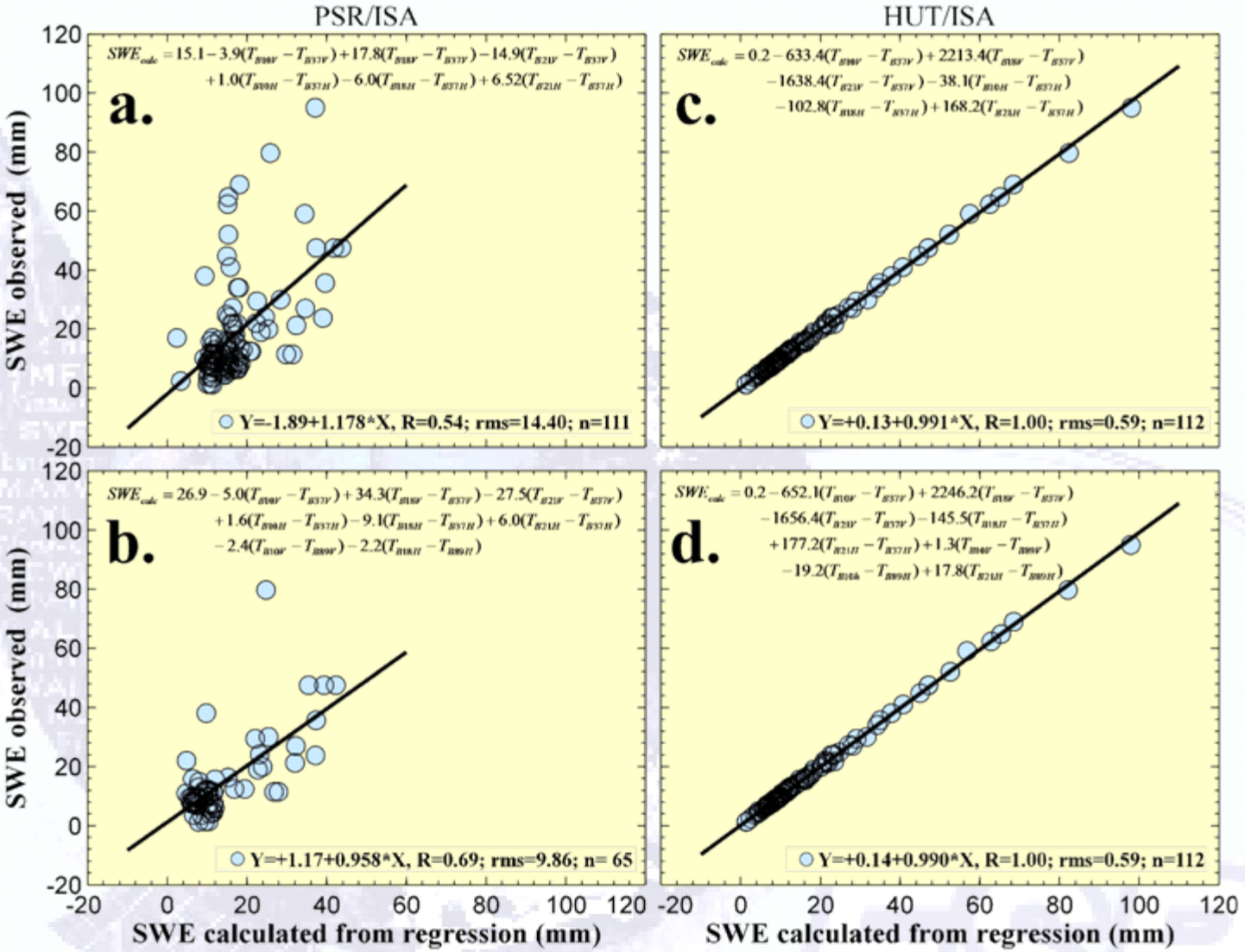

Correlation Analysis for All Data

- To obtain SWE images of the entire PSR covered MSAs that contained such diverse snowpacks, we also obained regression coefficients for the entire 2304 points colocation data set.

Each grid point was then tested for the land cover and

- **If the land cover contained no macro vegetaton the multiple regression coefficients obtained from the 224 points filtered dataset were used**

- **If not, the multiple regression coefficients obtained from the complete 2304 points dataset were used.**

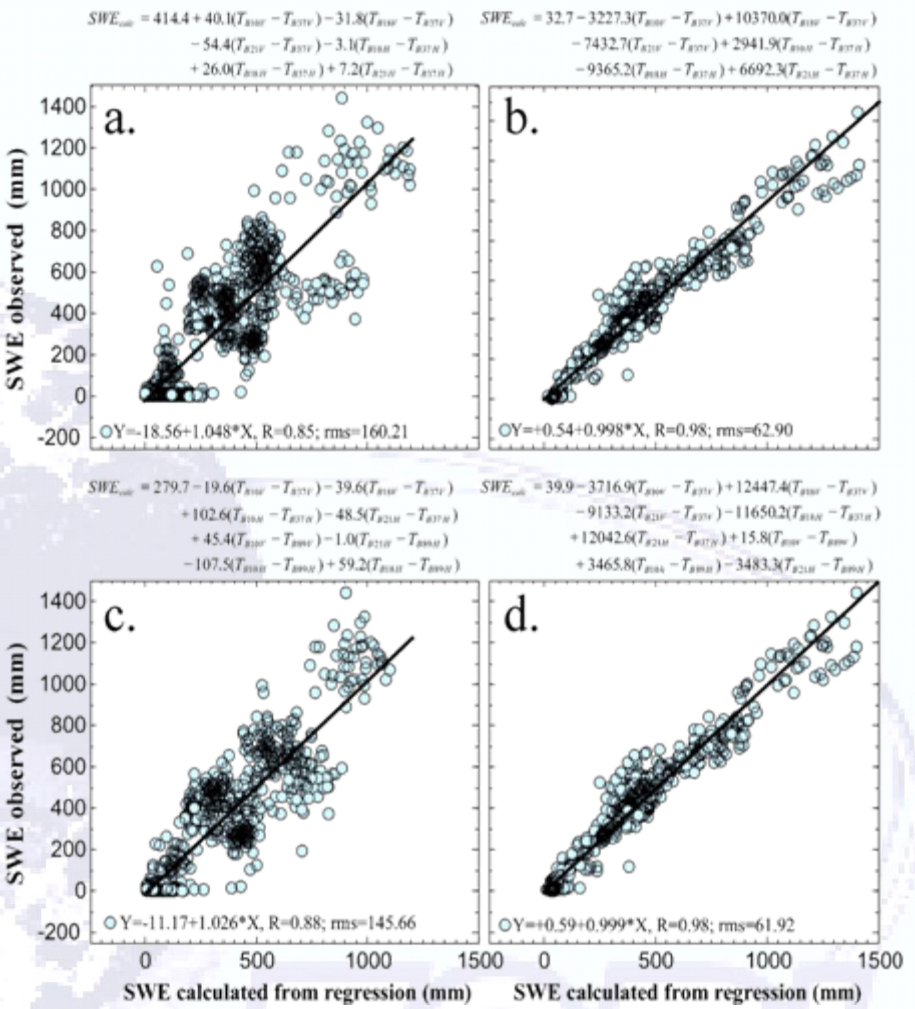

Computed SWE using Eqs. 1 and 2

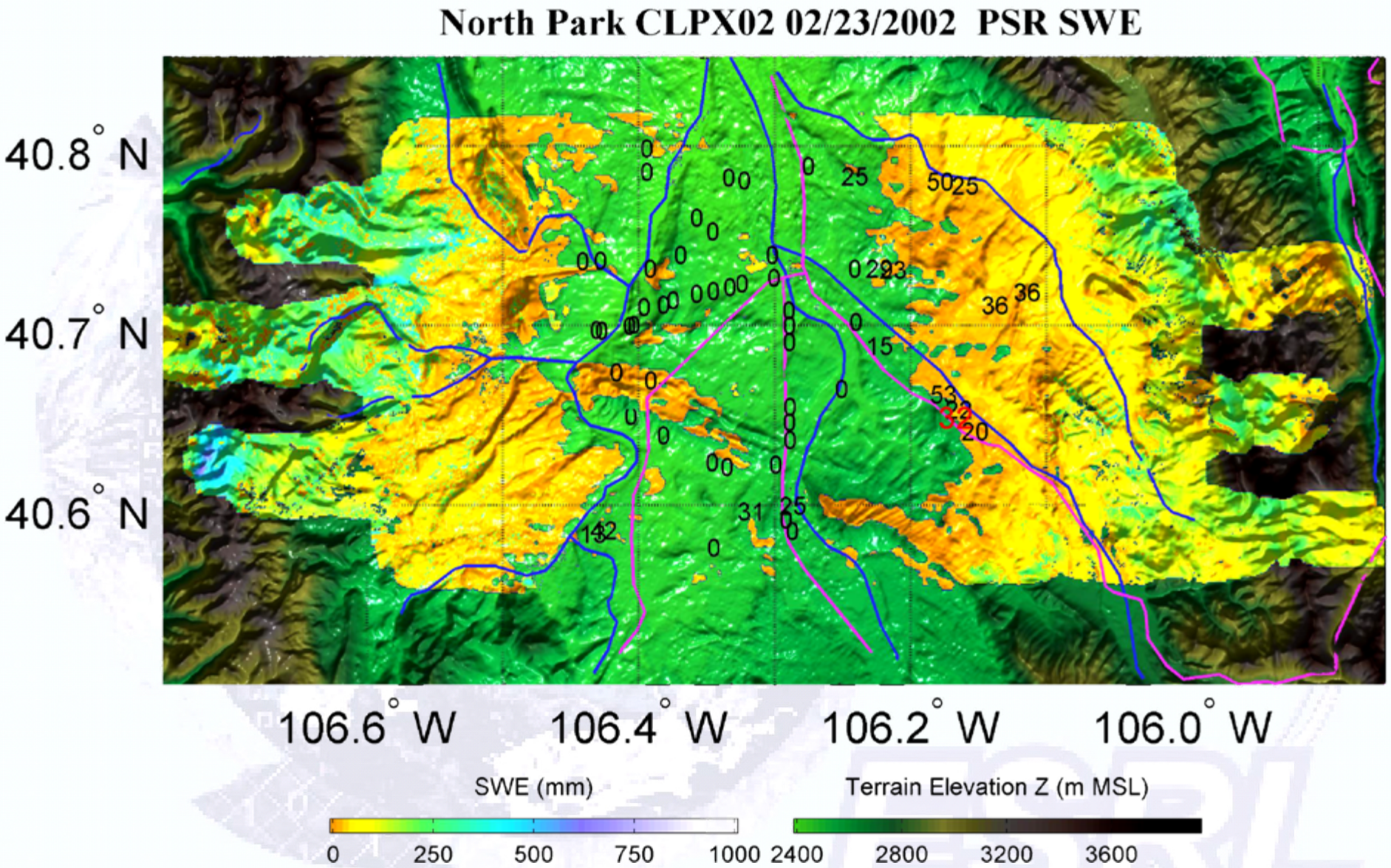

Computed SWE using Eqs. 1 and 2

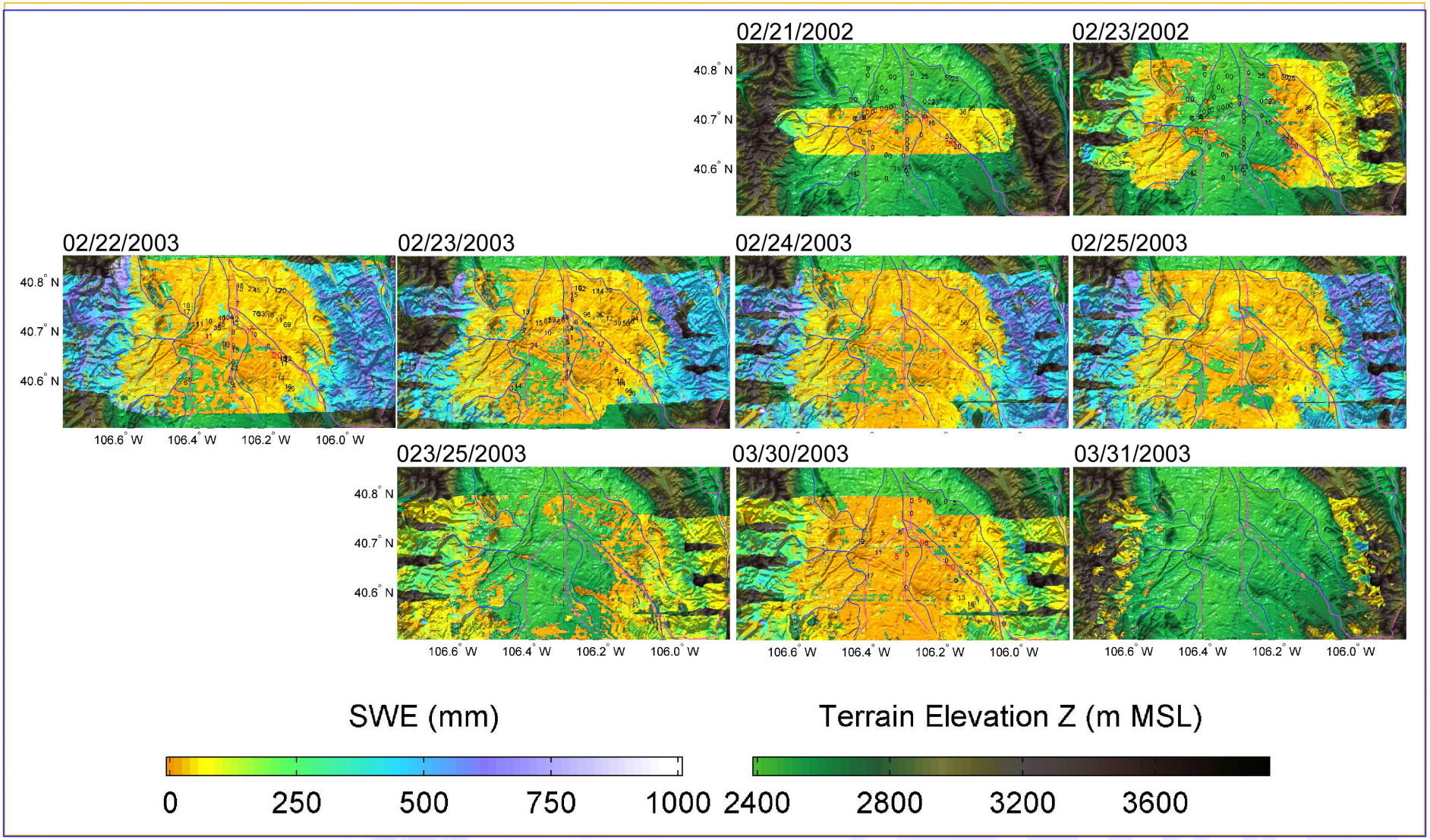

Computed SWE using Eqs. 1 and 2

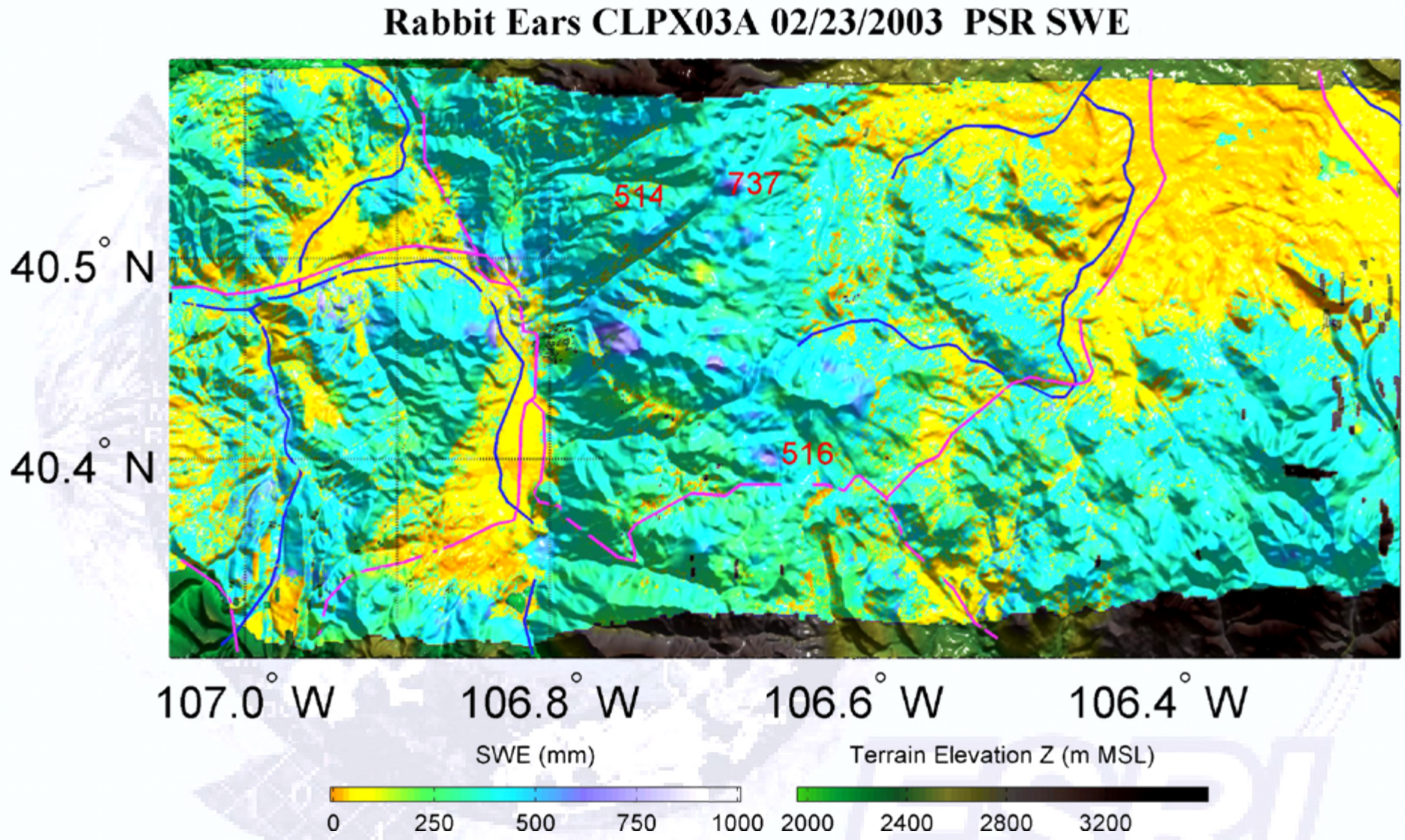

Computed SWE using Eqs. 1 and 2

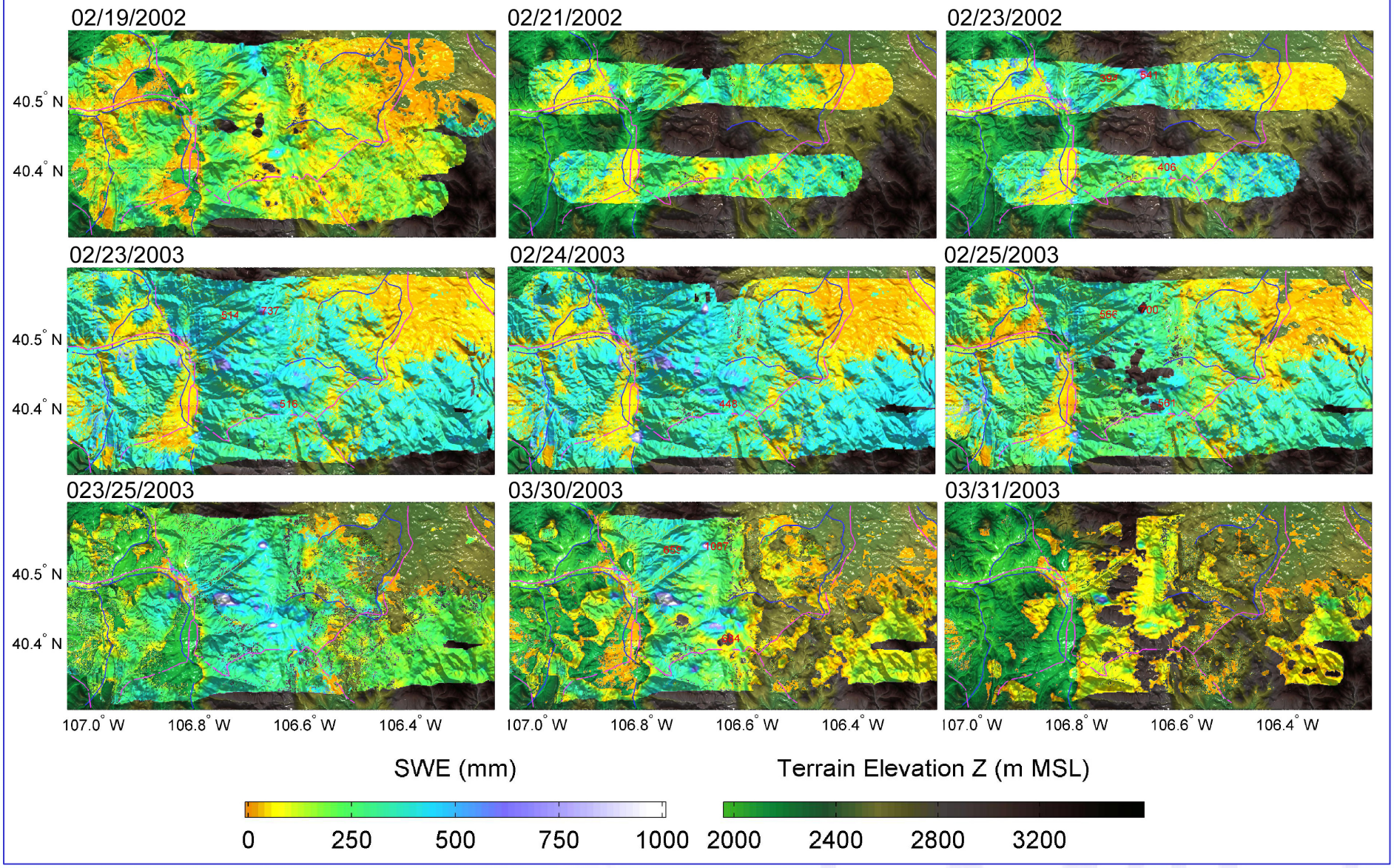

Computed SWE using Eqs. 1 and 2

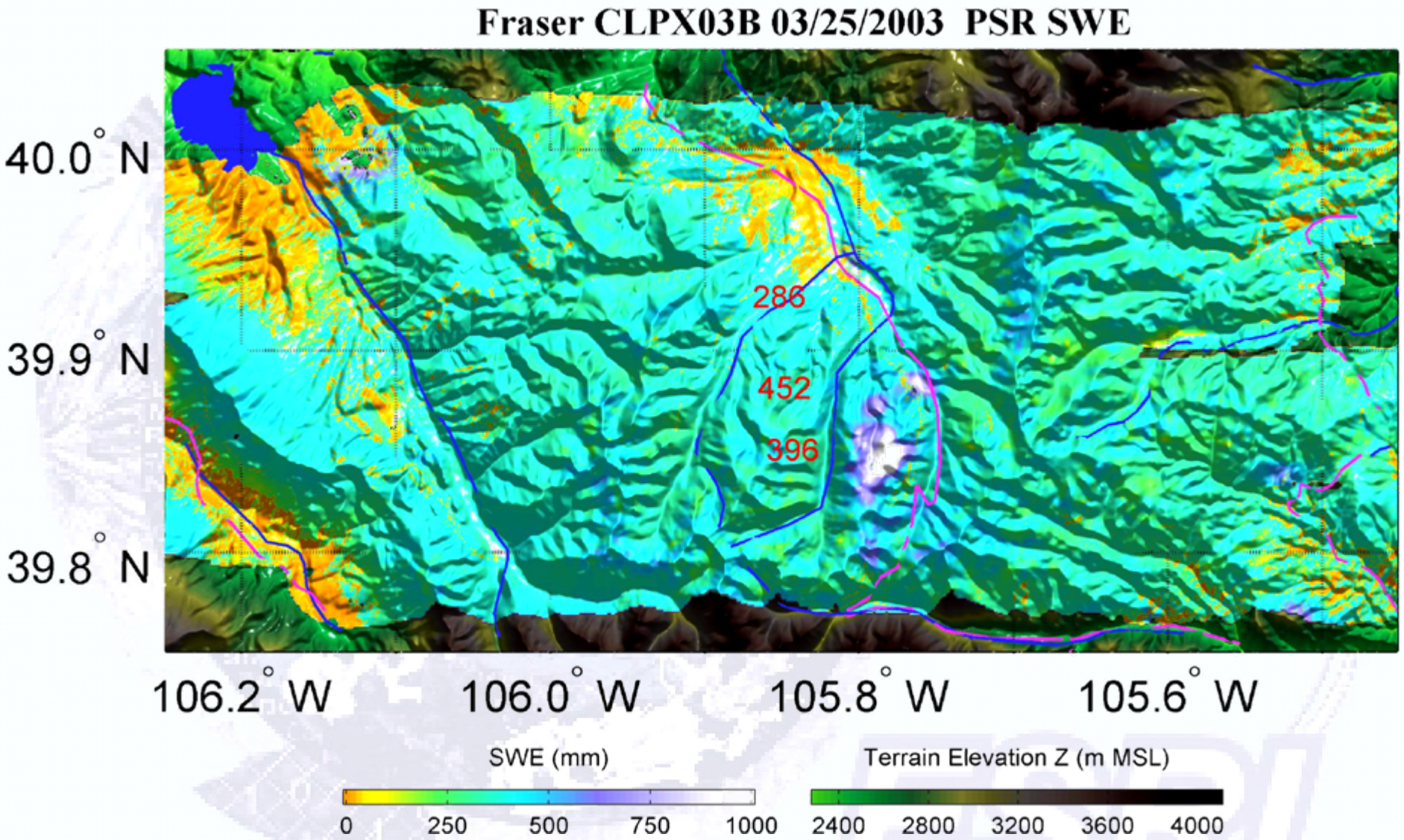

Computed SWE using Eqs. 1 and 2

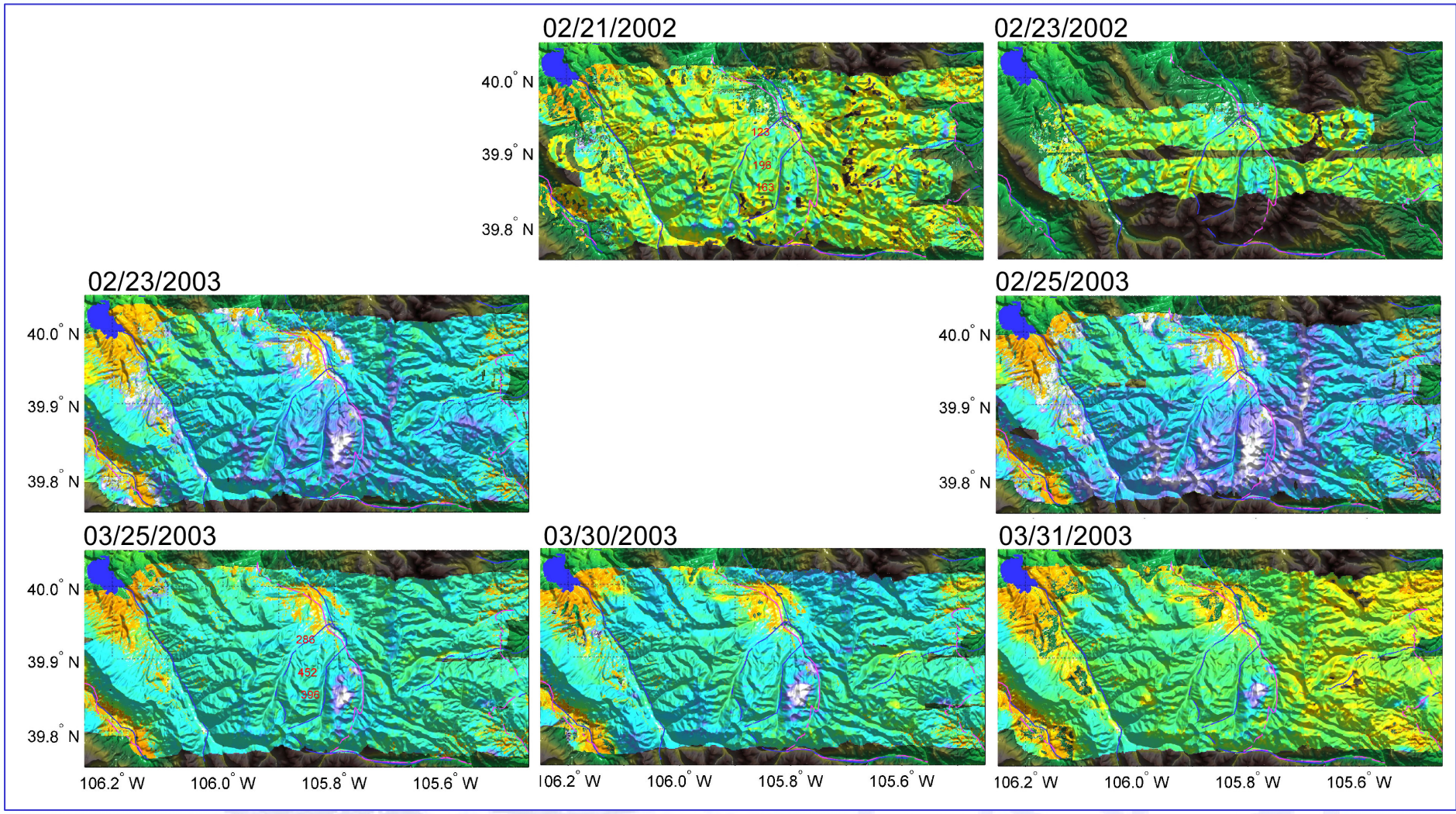

PSR/AMSR-E Comparison

AMSR-E Observations During CLPX

18 GHz

Feb. 2003

Mar. 2003

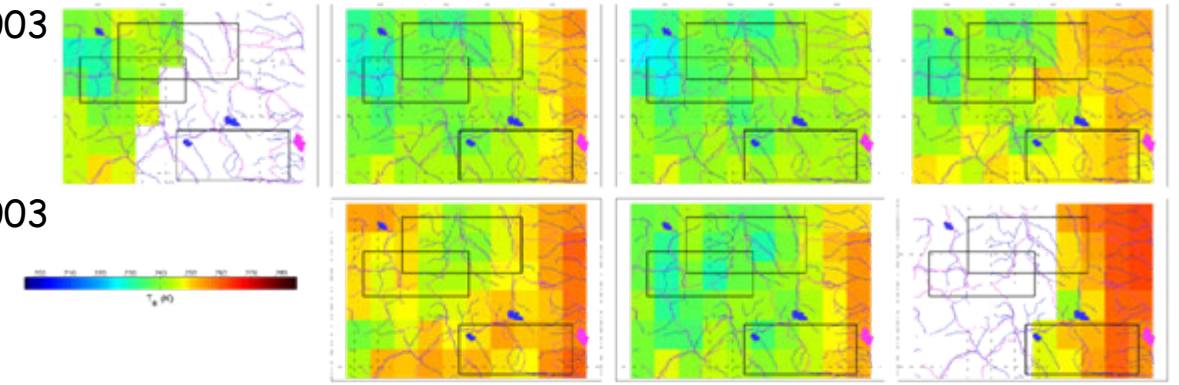

36 GHz

Feb. 2003

Mar. 2003

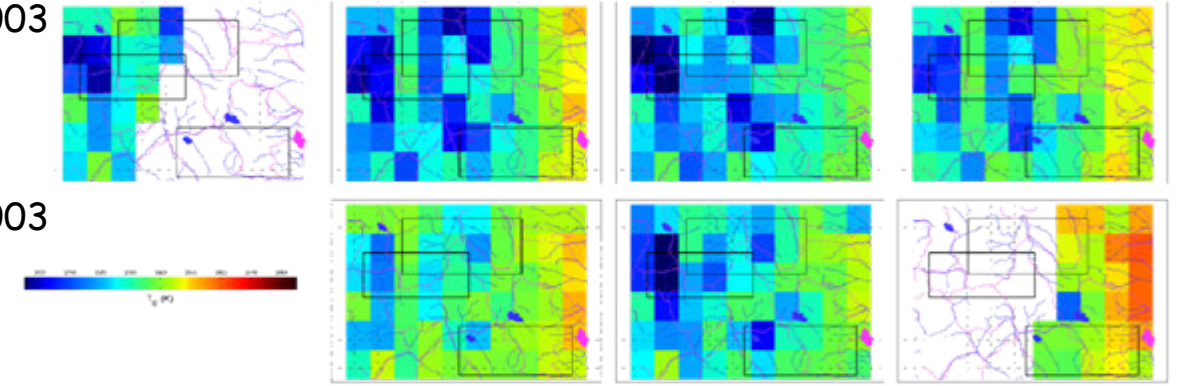

SWE
(Chang formula)

Feb. 2003

Mar. 2003

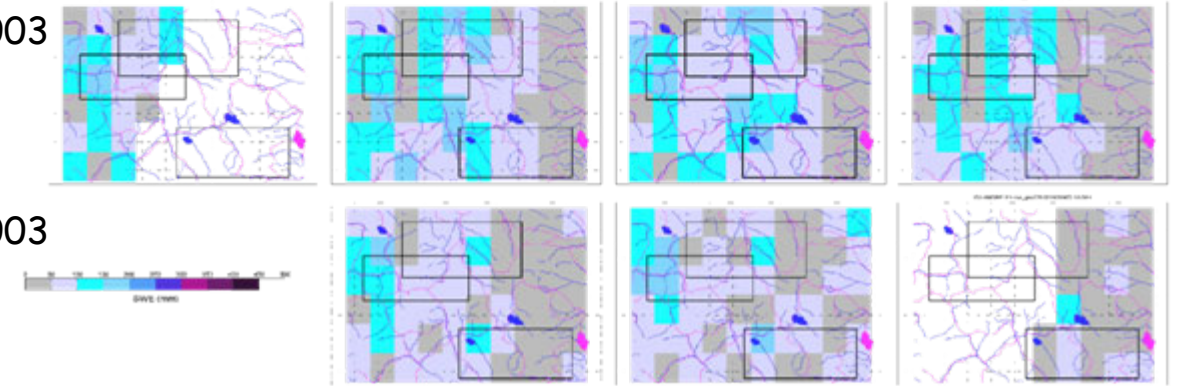

25 March 2003 PSR & AMSR-E Observations

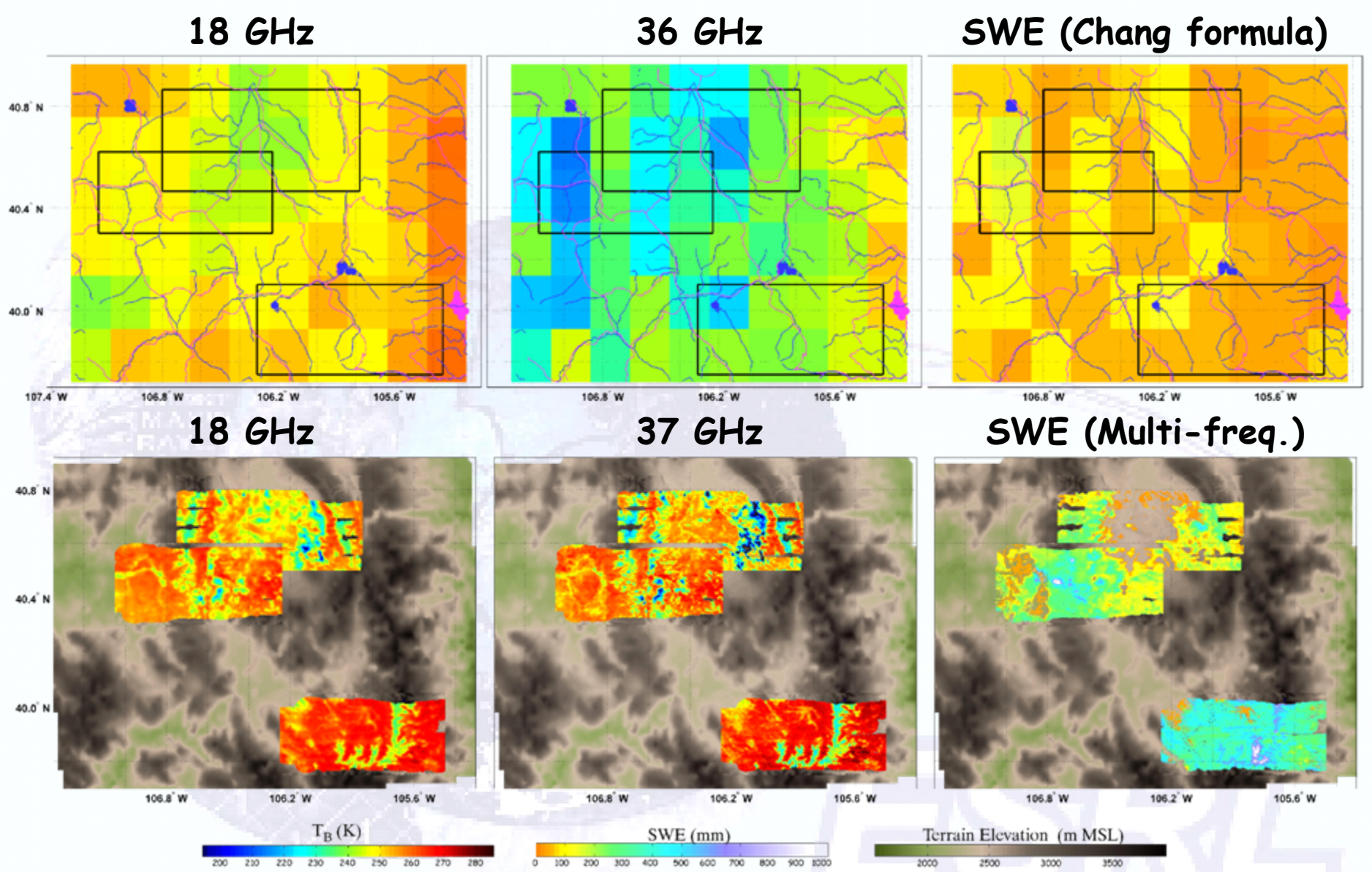

Improving AMSR-E SWE Retrieval

AMSR-E SWE (Chang formula) drapped over the 1-km terain elevation

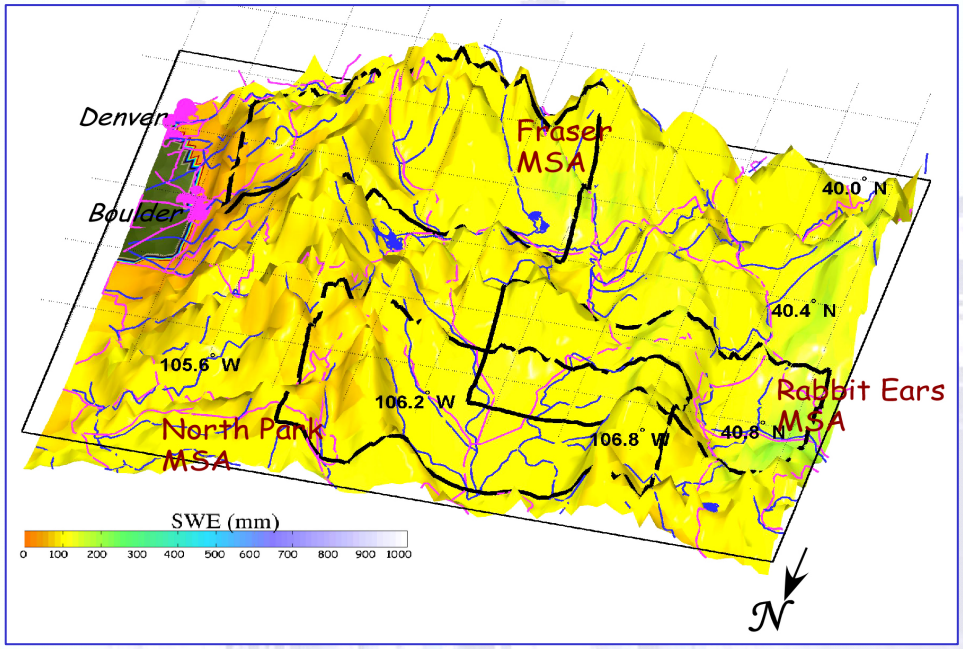

USGS 1-km resolution Land Cover data

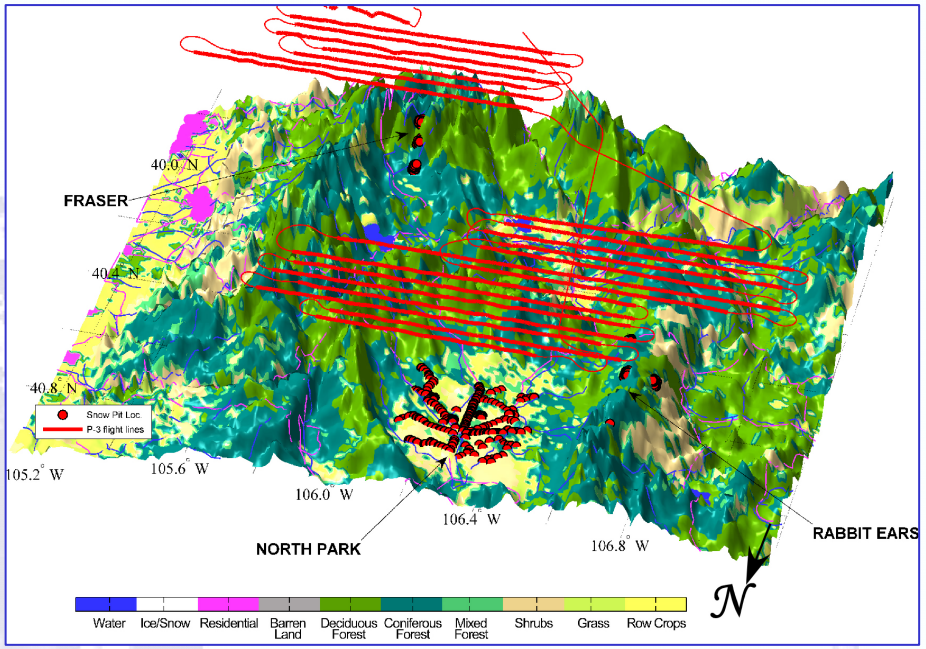

PSR/AMSR-E Comparison suggests that:

- Regional "calibration" using well designed experiments to compute multi-frequency regression algorithm could lead to applying those algorithms to the AMSR-E observations together with the land cover information and obtain more accurate global SWE information.

Summary

- We developed and analyzed a uniquely large and diverse data set of coincident observed and modeled microwave T_B data and *in situ* snow observations.
- Our results showed a strong frequency dependence of SWE as well as a high sensitivity to other snowpack properties that is consistent with past studies.
- When constrained to uniform dry snow conditions, the observed data strongly resemble theoretical T_B response.
- We developed multi-frequency algorithms for dry snow that resulted in RMS error of 14 mm, and when 89 GHz data were included RMS error was reduced to 10 mm.
- Multi-frequency algorithm for all data resulted in RMS error of 160 mm and when 89 GHz was added the RMS error was reduced to 145 mm
- SWE images were obtained for the PSR-covered MSAs using the multi-frequency algorithm for both dry dataset and the entire dataset.
- The mean *in situ* SWE observations show good agreement with the SWE computed with the multi-frequency algorithms.
- We suggest that regional "calibration" using well designed PSR experiments could lead to the improved SWE estimates from the AMSR-E observations.